

Monogamy of Mutual Information in Graph States

Jesus Fuentes,^a Cynthia Keeler,^a William Munizzi,^b and Jason Pollack^{c,d}

^a*Department of Physics, Arizona State University,
Tempe, AZ 85281, USA*

^b*Division of Physical Sciences, College of Letters and Science, University of California,
Los Angeles*

^c*Department of Electrical Engineering and Computer Science, Syracuse University, NY
13210, USA*

^d*Institute for Quantum & Information Sciences, Syracuse University, NY 13210, USA*
*E-mail: jesusfuentesun@gmail.com, keelerc@asu.edu,
wmunizzi17@ucla.edu, jasonpollack@gmail.com*

ABSTRACT: The monogamy of mutual information (MMI) is a quantum entropy inequality that enforces the non-positivity of tripartite information. We investigate the failure of MMI in graph states as a forbidden-subgraph phenomenon, conjecturing that every MMI-violating graph state is local-Clifford equivalent to one whose graph contains a four-star subgraph. We construct a family of star-like graphs whose states fail a specific class of MMI instances, and extend this analysis to general star topologies. Deriving adjacency matrix constraints that fix the MMI evaluation for these instances and interpreting them physically, we prove the forbidden-subgraph conjecture for this family of graphs. Finally, through an exhaustive search over graph representatives for all 8-qubit stabilizer entropy vectors, we establish that MMI failure is not reducible to the cases within our scope.

Contents

1	Introduction	1
2	Review	3
2.1	Entropy Vectors	3
2.2	Entropy Inequalities and Monogamy of Mutual Information	3
2.3	Stabilizer States and the Tableau Formalism	4
2.4	Graph States	6
3	MMI Failure in Tableaux and Graphs	7
3.1	Tableaux and MMI	7
3.2	Entanglement Entropies From the Adjacency Matrices	10
4	Conditions for MMI Violation in Graph States	15
4.1	An MMI-Violating Graph	16
4.2	Characterization of MMI Family Violation in a Larger Family of Graph States	19
4.3	A Physical Interpretation of the MMI_{CIJ} Violation Conditions	25
4.3.1	From Column Spaces to Reachable Circuits	25
4.3.2	The Physical Meaning of a Nontrivial Intersection	26
4.3.3	The Physical Meaning of Distributivity	27
4.4	MMI Failure for $ \mathcal{G}\rangle$ states is Not Fully Reducible to MMI_{CIJ} Failure	28
5	Discussion: Toward a Complete Characterization of MMI Violation in Stabilizer States	31
A	Additional Derivations and Proofs	36
A.1	Expressing MMI_{CIJ} as the Dimension of Column Spaces of Adjacency Submatrices	36
A.2	A Classification of $ \mathcal{G}\rangle$ According to MMI Evaluation Based on the Properties of the Block Elements of $\Gamma^{\mathcal{L}}$	36
A.3	Deducing the Claims in Section 4.3	38
A.4	Graph Representatives for Every Stabilizer State Entropy Vector at $n = 8$ Qubits, up to Symmetry, and Their MMI Evaluations	39
B	MMI Failure in Stabilizer States	47
B.0.1	Three Qubits	47
B.0.2	Four Qubits	47
B.0.3	Five Qubits	48
B.0.4	Six Qubits	52

1 Introduction

An important insight from quantum information theory is that entanglement is fully characterized by not just a single numerical value, but also by *how* it is distributed among the constituent parties of a quantum state. In multipartite systems, this pattern of entanglement precisely constrains how information can be stored, transmitted, and processed using the state [1]. Entanglement monotones [2, 3], such as entanglement entropy, quantify and bound the overall strength of bipartite correlations; however, the entanglement structure of a state is further restricted by sets of fundamental inequalities which dictate how quantum information can be shared across the different subsystems [4, 5]. Among these, the best known are the subadditivity [6] and strong subadditivity [7, 8] inequalities, which are satisfied by all quantum states. Beyond these universal quantum inequalities, additional constraints exist [9–16] which are only satisfied by particular classes of states, reflecting the specialized features of those states.

One particularly intriguing constraint, satisfied only by a limited subset of quantum states, is the monogamy of mutual information (MMI) inequality [17]

$$I(A : BC) \geq I(A : B) + I(A : C), \quad (1.1)$$

which imposes strong restrictions on the entanglement patterns that states can exhibit. A prominent example of states that obey MMI is the class of holographic states, the set of quantum states which are dual to classical holographic systems via the AdS/CFT correspondence [18]. In a system of entangled qubits, MMI dictates how information can be distributed among the qubits, while maintaining maximal bipartite entanglement between specific pairs. Consequently, understanding the conditions under which MMI is violated has emerged as an active area of contemporary research [19–21], with implications ranging from insights into spacetime reconstruction [22] in quantum gravity to enhanced protocols for distributed computation [23, 24] in quantum networks.

Generic quantum states, and even states with relatively “simple” entanglement patterns, fail MMI. In fact, MMI failure occurs at small system sizes ($n = 4$) even among stabilizer states [25], the class of quantum states well known to be efficiently simulable [26] on a classical computer. A canonical example is the 4-qubit *GHZ* state, a stabilizer state whose entanglement entropy is the same regardless of the Hilbert space partition.

The full set of entanglement structures achievable by stabilizer states can be realized on a strict subset [27], the set of graph states. In the graph state formalism [23, 24, 28–31], each state is represented as a simple undirected graph, where vertices correspond to qubits and edges encode the action of CZ gates. This representation provides a natural framework for analysis of MMI violations in stabilizer states, using the graph-theoretic encoding of entanglement in graph states.

In this paper, we translate the evaluation of MMI for stabilizer states into an analysis of connectivity in graph states. We identify the algebraic conditions on graph adjacency matrices that determine the entanglement structures for the corresponding states, and consequently determine whether each entanglement structure satisfies or fails MMI. We discover a family of graphs that are guaranteed to fail MMI, and characterize the physical features of the states they represent. Furthermore, we specify conditions that give rise to MMI violation, highlighting minimal structural features responsible for such failures and describing how multipartite correlations depend on the graph topology. By understanding when and why violations of MMI occur, we gain deeper insight into the entanglement structures for different state classes, as well as into the physical properties which determine their potential utility in quantum information science.

The remainder of this paper is organized as follows. In Section 2, we review the stabilizer formalism and define the mapping between stabilizer entanglement entropies and graph state connectivity. In Section 3 we demonstrate how MMI can be reformulated as a comparison between graph adjacency matrices, and define MMI violation as a forbidden-subgraph problem. Section 4 specifies precise conditions under which MMI is violated in stabilizer states, using our graph-theoretic formalism. In Section 5 we discuss the impact of this work, and propose future follow-ups to this manuscript.

A comprehensive set of appendices accompanies this work, providing an extensive catalog of stabilizer state entanglement structures. These appendices include graph representations for all stabilizer state entropy vectors up through $n = 8$ qubits, detailed MMI evaluations for each entropy vector, and physical interpretations corresponding to each entanglement structure. We further provide the count and percentages of stabilizer states which satisfy, saturate, and fail MMI at each qubit number, offering a self-contained reference for future studies of entanglement in stabilizer and graph states. The appendices also include full derivations, proofs, and added details for the calculations in this work. In particular, Tables 11–13 provide graph representatives for every unique entropy vector at $n = 8$, along with hyperlinks to a website that gives direct access to the entropy vector of the corresponding state.

2 Review

2.1 Entropy Vectors

Given a factorizable Hilbert space \mathcal{H} , and n -party pure state $|\psi\rangle \in \mathcal{H}$, let I denote an ℓ -party subsystem of $|\psi\rangle$. The entanglement entropy S_I , between I and its $(n-\ell)$ -party complement \bar{I} is computed as

$$S_I = -\text{Tr}(\rho_I \log(\rho_I)), \quad (2.1)$$

with ρ_I the reduced density matrix of subsystem I . Since we will consider qubit systems in this paper, it is natural for information to be measured in bits, and entropies are therefore computed using \log_2 .

For a fixed division of the Hilbert space into n parties, there are $2^n - 1$ computable entanglement entropies of a state $|\psi\rangle$. The ordered list of these entropies forms the entropy vector [19] for $|\psi\rangle$, and contains a complete description of the state's bipartite entanglement structure. For example, a 3-party state $|\psi\rangle$ has an entropy vector

$$\vec{S}(|\psi\rangle) = (S_A, S_B, S_C, S_{AB}, S_{AC}, S_{BC}, S_{ABC}). \quad (2.2)$$

For a pure state $|\psi\rangle$, the fact that $S_{ABC} = 0$ and $S_I = S_{\bar{I}}$ gives a symmetry to the entropy vector $\vec{S}(|\psi\rangle)$. This symmetry allows $\vec{S}(|\psi\rangle)$ to be specified using only $2^{n-1} - 1$ components, for example

$$\vec{S}(|\psi\rangle) = (S_A, S_B, S_C). \quad (2.3)$$

Since we are considering pure states in this paper, we often use this reduced entropy vector notation for compactness.

2.2 Entropy Inequalities and Monogamy of Mutual Information

A homogeneous entropy inequality is a linear constraint of the form

$$\sum_{\emptyset \neq A \in [n]} b_A S_A \geq 0 \quad b_A \in \mathbb{Z}, \quad (2.4)$$

that restricts the entanglement structure for a class of quantum states. The closure of the set of all entropy vectors of the class of states obeying some inequalities defines a convex, polyhedral subspace of the entropy vector space, known as the entropy cone [9, 19, 32]. Accordingly, all entropy vectors realized by states in a particular class must reside within the entropy cone for that class. One such inequality, obeyed by all quantum states dual to classical holographic systems [17], is the monogamy of mutual information (MMI). For an n -party system with pairwise-disjoint subsystems I , J , and K , MMI requires

$$S_{IJ} + S_{IK} + S_{JK} \geq S_I + S_J + S_K + S_{IJK}. \quad (2.5)$$

We will refer to a single MMI instance, specified by pairwise disjoint tripartite subsystems I, J, K , as MMI_{IJK} . When discussing MMI in general, which constitutes all inequalities of the form of Eq. (2.5), we will omit this notation and simply refer to “MMI.” In a purely quantum-information context, MMI defines the non-positivity of tripartite information and constrains the correlations that can be shared among three parties while retaining maximal entanglement between any two. The MMI inequalities in Eq. (2.5), ranging over all possible choices of disjoint subsystems I, J, K , constitute a collection of inequalities obeyed by the holographic entropy cone [19].

2.3 Stabilizer States and the Tableau Formalism

The Pauli group on n qubits, denoted \mathcal{P}_n , is the set of all n -fold tensor products of Pauli operators (including global phases), explicitly

$$\mathcal{P}_n = \left\{ i^j \sigma_1 \otimes \sigma_2 \otimes \cdots \otimes \sigma_n \mid j \in \{0, 1, 2, 3\}, \sigma_k \in \{\mathbb{1}, \sigma_x, \sigma_y, \sigma_z\} \right\}, \quad (2.6)$$

where each Pauli operator admits a 2×2 matrix representation as

$$\mathbb{1} = \begin{bmatrix} 1 & 0 \\ 0 & 1 \end{bmatrix}, \quad \sigma_x = \begin{bmatrix} 0 & 1 \\ 1 & 0 \end{bmatrix}, \quad \sigma_y = \begin{bmatrix} 0 & -i \\ i & 0 \end{bmatrix}, \quad \sigma_z = \begin{bmatrix} 1 & 0 \\ 0 & -1 \end{bmatrix}. \quad (2.7)$$

Given \mathcal{P}_n , the n -qubit stabilizer states [26] are then defined as the set of states invariant under a 2^n -element subgroup of \mathcal{P}_n . Alternatively, the n -qubit stabilizer states can be defined as the orbit [33] of $|0\rangle^{\otimes n}$ under the n -qubit Clifford group \mathcal{C}_n . The Clifford group is the normalizer of \mathcal{P}_n in $U(2^n)$,

$$\mathcal{C}_n \equiv \{U \in U(2^n) \mid U\mathcal{P}_nU^\dagger \subseteq \mathcal{P}_n\}. \quad (2.8)$$

The group \mathcal{C}_n is generated by the Hadamard H , phase P , and Controlled-NOT¹ $CNOT$ quantum gates, each representable by the following matrices

$$H = \frac{1}{\sqrt{2}} \begin{bmatrix} 1 & 1 \\ 1 & -1 \end{bmatrix}, \quad P = \begin{bmatrix} 1 & 0 \\ 0 & i \end{bmatrix}, \quad CNOT_{1,2} = \begin{bmatrix} 1 & 0 & 0 & 0 \\ 0 & 1 & 0 & 0 \\ 0 & 0 & 0 & 1 \\ 0 & 0 & 1 & 0 \end{bmatrix}. \quad (2.9)$$

Representing a generic qubit state requires an exponential number of classical bits to account for the 2^n Hilbert space dimension. Famously, however, each n -qubit stabilizer state can be described using $\mathcal{O}(n^2)$ classical bits, and Clifford circuits acting on stabilizer states are therefore efficiently classically simulable [25, 26]. This substantial reduction in the overhead is exhibited by the tableau formalism, an efficient representation for stabilizer states and Clifford transformations. Let $\mathfrak{G} = \{g_1, \dots, g_n\}$ be the generating set for the stabilizer subgroup $S < \mathcal{P}_n$ of a state

¹We use a convention for $CNOT_{i,j}$ where i denotes the control qubit and j the target qubit.

$|\psi\rangle$. We represent \mathfrak{G} , and thereby the state $|\psi\rangle$, as a pair of binary square matrices $X, Z \in \mathbb{Z}_2^{n \times n}$ with entries defined

$$X_{ij} = \begin{cases} 1, & (g_i)_j \in \{\sigma_x, \sigma_y\} \\ 0, & \text{otherwise} \end{cases} \quad Z_{ij} = \begin{cases} 1, & (g_i)_j \in \{\sigma_y, \sigma_z\} \\ 0, & \text{otherwise} \end{cases} \quad (2.10)$$

where $(g_i)_j$ indicates the j^{th} operator in the Pauli string g_i and $\mathbb{Z}_2 = \{0, 1\}$. Placing the matrices X and Z side-by-side gives the $n \times 2n$ tableau representation for $|\psi\rangle$:

$$T_\psi = [X \mid Z]. \quad (2.11)$$

To uniquely specify a state, we also need to assign a sign ± 1 to each row in T_ψ . However, since this specification does not impact the entanglement entropy of the state, we will omit it.

The evolution of $|\psi\rangle$ under Clifford operators can likewise be efficiently simulated through simple transformations on T_ψ . For each n -qubit Clifford operator, the associated action on T_ψ is described by a map

$$T_\psi \mapsto T'_\psi = [X' \mid Z'], \quad (2.12)$$

implemented through bitwise XOR (\oplus) operations on the affected columns. For the Hadamard, phase, and $CNOT$ gates the respective update rules [25, 26] on each row $i \in n$ in T_ψ are

$$H_a : \quad X'_{ia} = Z_{ia}, \quad Z'_{ia} = X_{ia}; \quad (2.13)$$

$$S_a : \quad X'_{ia} = X_{ia}, \quad Z'_{ia} = Z_{ia} \oplus X_{ia}; \quad (2.14)$$

$$CNOT_{a,b} : \quad X'_{ib} = X_{ib} \oplus X_{ia}, \quad Z'_{ia} = Z_{ia} \oplus Z_{ib}. \quad (2.15)$$

All other tableau entries (except possibly those specifying the signs of rows) remain unchanged. Eqs. (2.13)–(2.15) are applied sequentially each time the corresponding gate acts on $|\psi\rangle$.

The entanglement entropies of a state $|\psi\rangle$ can likewise be computed from the tableau T_ψ . For an n -party state $|\psi\rangle$, let $A \subseteq \{n\}$ denote the A subsystem and P_A the projection operator that deletes every column of X and Z in T_G indexed by \bar{A} . The entanglement entropy of A with \bar{A} is then calculated [30] as

$$S_A(|\psi\rangle) = R_A - |A|, \quad (2.16)$$

where $R_A \equiv \text{rank}_{\mathbb{Z}_2}(P_A(T_G))$. Eq. (2.16) therefore offers an efficient technique for evaluating stabilizer entanglement entropies using the tableau formalism.

2.4 Graph States

A graph state is a quantum state representable by a simple, undirected graph, where vertices indicate qubits and edges indicate CZ action. Since the CZ gate acting on the state $|+\rangle$ generates maximal entanglement, the edges of a graph state additionally encode the entanglement structure of the state. Given a graph $G = (V, E)$ with n vertices, the corresponding graph state $|G\rangle$ is obtained by acting on the all-plus state $|+\rangle^{\otimes n}$ with a controlled- Z gate for each edge in G , explicitly

$$|G\rangle = \prod_{(i,j) \in E} CZ_{i,j} |+\rangle^{\otimes n}. \quad (2.17)$$

In terms of Clifford generators, $CZ_{i,j} = H_j CNOT_{i,j} H_j$. The CZ gate is symmetric, making the distinction between control and target qubits purely conventional.

A local Clifford (LC) operation is a Clifford operator that acts as a non-identity only on a single qubit. On a graph state $|G\rangle$, LC operations can be realized [27] as a local complementation on the associated graph G . Accordingly, we use LC to refer interchangeably to local Clifford equivalence and local complementation equivalence in graph states. For a graph G and vertex a , the local complementation τ_a acts on the open neighborhood of a (i.e. the neighborhood of a with a itself excluded) in G , denoted $N(a)$. The transformation τ_a replaces the subgraph of G , induced² by $N(a)$, with its graph complement. The graphical effect of local complementation is illustrated by Figure 1.

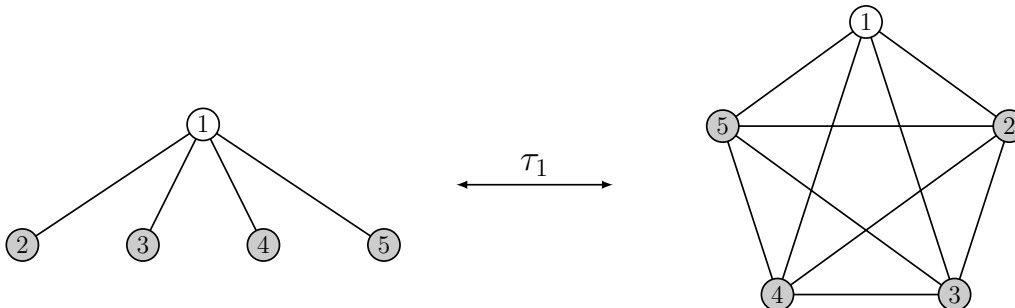


Figure 1. Left: star graph on five vertices K_5 . Right: the result of locally complementing K_5 on vertex 1, a complete graph on five vertices. The neighborhood of vertex 1, $N(1)$, is shaded in both cases. Notice that locally complementing vertex 1 of the complete graph recovers K_5 .

The effect of τ_a on the adjacency matrix for G is

$$\tau_a(\Gamma_G) = \Gamma_G + \Gamma_{N(a)} \pmod{2}, \quad (2.18)$$

²Recall that the subgraph of a graph $G = (V, E)$ induced by the vertex set $V' \subseteq V$ is the graph with vertices V' and edges connecting two vertices in V' if and only if those vertices are connected by an edge in G .

where $\Gamma_{N(a)}$ is the adjacency block of Γ_G corresponding to $N(a)$.

Each stabilizer state can be mapped to a graph state under LC operations [27]. Moreover, since LC operations are single-qubit unitaries, they preserve all binary entanglement entropies and thus the entropy vector. For this reason stabilizer and graph states share the same set of entropy vectors, despite graph states comprising a proper subset of the stabilizer states, thereby motivating our exploration of the stabilizer entropy cone using graph states.

Entanglement entropies in graph states can be computed directly from the adjacency matrix [23, 34]. For a graph G with vertex set $V = \{n\}$ and adjacency matrix Γ_G , let $\{A, \bar{A}\}$ be any bipartition of V . The entanglement entropy of A , in $|G\rangle$, is calculated from Γ_G as

$$S_A(|G\rangle) = \text{rank}_{\mathbb{Z}_2} \left(\Gamma_G^{A, \bar{A}} \right). \quad (2.19)$$

The matrix $\Gamma_G^{A, \bar{A}}$ in Eq. (2.19) indicates the local information submatrix of A , extracted from Γ_G by only considering edges connecting a vertex in A with a vertex in \bar{A} . Explicitly, we define $\Gamma_G^{A, \bar{A}}$ as

$$\Gamma_G^{A, \bar{A}} = \left[(\Gamma_G)_{ij} \right]_{i \in A, j \in \bar{A}}. \quad (2.20)$$

While the local information submatrix $\Gamma_G^{A, \bar{A}}$ contains the information needed to compute the entanglement entropy for any subsystem of $A' \subseteq A$, $S_{A'}$ is independent of the matrix square blocks corresponding to the self adjacencies of A' and \bar{A}' .

Going forward we omit the subscript on $\Gamma_G^{A, \bar{A}}$, as context will unambiguously identify the associated graph. We likewise omit the complement subsystem in the superscript for conciseness.

3 MMI Failure in Tableaux and Graphs

In this section, we show that the monogamy of mutual information (MMI) inequalities can be reformulated as a comparison between the ranks of tableau submatrices. We further demonstrate how the entangling action of a $CNOT$ gate alters the row and column spaces of these submatrices, thereby changing their ranks and leading to MMI violation. Extending this construction, we move to a graph-theoretic formulation in which MMI violation exists as a forbidden-subgraph problem. Using graph state adjacency submatrices, which encode the entanglement connectivity between distinct subsystems, we qualify the conditions required for MMI violation.

3.1 Tableaux and MMI

The monogamy of mutual information (MMI) inequalities, given in Eq. (2.5), are typically expressed in terms of subsystem entanglement entropies S (2.1). However, when a state $|\psi\rangle$ admits a tableau representation, MMI can be reformulated directly

in terms of the tableau data. For a stabilizer state $|\psi\rangle$ with associated tableau T_ψ , we can use Eq. (2.16) to rewrite MMI using the ranks of the corresponding tableau projections as

$$R_{IJ} + R_{IK} + R_{JK} \geq R_I + R_J + R_K + R_{IJK}. \quad (3.1)$$

The expression of MMI in Eq. (3.1) offers a useful algebraic format to better analyze stabilizer entanglement structure. In particular, rewriting MMI in terms of submatrix ranks allows us to analyze how a sequence of quantum gates, via transformations on the tableau, induces a violation of MMI by directly altering the linear dependencies of tableau submatrices.

As a preliminary example, we use Eq. (3.1) to analyze how a single Clifford gate induces the MMI failure exhibited by the four-qubit GHZ , the lowest qubit number stabilizer state to violate an MMI (2.5) instance. The four-qubit GHZ can be prepared using Clifford generators as

$$|GHZ\rangle_4 = CNOT_{3,4}CNOT_{3,2}CNOT_{3,1}H_3|0\rangle^{\otimes 4} = \frac{1}{\sqrt{2}}(|0000\rangle + |1111\rangle), \quad (3.2)$$

and has a stabilizer group

$$\text{Stab}(|GHZ\rangle_4) = \langle XXXX, ZZII, IZZI, IIZZ \rangle. \quad (3.3)$$

To perform our analysis, we consider the state

$$|\phi\rangle = CNOT_{3,4}|GHZ\rangle_4 = \frac{1}{\sqrt{2}}(|0000\rangle + |1110\rangle), \quad (3.4)$$

with stabilizer group

$$\text{Stab}(|\phi\rangle) = \langle XXXI, ZZII, IZZI, IIIZ \rangle. \quad (3.5)$$

Acting with a single $CNOT_{3,4}$ gate transforms $|\phi\rangle$ back into $|GHZ\rangle_4$. The tableaux $T_{|GHZ\rangle_4}$ and $T_{|\phi\rangle}$ are presented in Table 1.

The state $|\phi\rangle$ has the entropy vector

$$\vec{S}(|\phi\rangle) = (1, 1, 1, 1, 1, 1, 0), \quad (3.6)$$

which saturates every 4-qubit instance of MMI (2.5). In contrast, $|GHZ\rangle_4$ has the entropy vector

$$\vec{S}(|GHZ\rangle_4) = (1, 1, 1, 1, 1, 1, 1), \quad (3.7)$$

which violates multiple instances of MMI (2.5), as shown in Table 1.

State	(1,2,3)	(1,2,4)	(1,3,4)	(2,3,4)	(1,2,34)
$ \phi\rangle$ (Before)	ST	ST	ST	ST	ST
$ GHZ\rangle_4$ (After)	F	F	F	F	ST

State	(1,3,24)	(1,4,23)	(2,3,14)	(2,4,13)	(3,4,12)
$ \phi\rangle$ (Before)	ST	ST	ST	ST	ST
$ GHZ\rangle_4$ (After)	ST	ST	ST	ST	ST

Table 1. Starting from state $|\phi\rangle$, which saturates all 4-qubit MMI instances, a single $CNOT_{3,4}$ transforms $|\phi\rangle$ into $|GHZ\rangle_4$, which fails MMI. Columns label the MMI instance, and show whether each state satisfies (S), saturates (ST), or fails (F) that instance.

We inspect the rank vector \vec{R} , the ordered set of tableau submatrix ranks, to understand how the application of $CNOT_{3,4}$ induces an MMI violation. Specifically, we focus our analysis on the 3-party MMI instance that involves subsystems $\{1, 2, 3\}$, $MMI_{\{1,2,3\}}$. Table 2 shows each component of $\vec{R}_{|\phi\rangle}$ and $\vec{R}_{|GHZ\rangle_4}$ that appears in $MMI_{\{1,2,3\}}$, and illustrates how the action of $CNOT_{3,4}$ selectively increases component R_{123} from 3 to 4, leading to violation.

State	R_1	R_2	R_3	R_{12}	R_{13}	R_{23}	R_{123}
$ \phi\rangle$ (Before)	2	2	2	3	3	3	3
$ GHZ\rangle_4$ (After)	2	2	2	3	3	3	4

Table 2. Rank vectors \vec{R} for $|\phi\rangle$ and $|GHZ\rangle_4$ (before and after $CNOT_{3,4}$ is applied). The action of $CNOT_{3,4}$ increments the R_{123} component of $\vec{R}_{|\phi\rangle}$ by 1, causing a violation of $MMI_{\{1,2,3\}}$, the MMI on the 3-party instance involving subsystems $\{1, 2, 3\}$.

The rank increase shown in Table 2 is generated by a change to the column space of the $|\phi\rangle$ tableau. Table 3 gives the tableaux for $|\phi\rangle$ and $|GHZ\rangle_4$, each projected onto the subsystem $\{123\}$ and its complement $\{4\}$. The objects T_{123} and T_4 represent the tableau submatrices for subsystems $\{123\}$ and $\{4\}$ respectively.

State	T_{123}	T_4
$ \phi\rangle$ (Before)	$\left[\begin{array}{ccc ccc} 1 & 1 & 1 & 0 & 0 & 0 \\ 0 & 0 & 0 & 1 & 1 & 0 \\ 0 & 0 & 0 & 0 & 1 & 1 \\ 0 & 0 & 0 & 0 & 0 & 0 \end{array} \right]$	$\left[\begin{array}{c c} 0 & 0 \\ 0 & 0 \\ 0 & 0 \\ 0 & 1 \end{array} \right]$
$ GHZ\rangle_4$ (After)	$\left[\begin{array}{ccc ccc} 1 & 1 & 1 & 0 & 0 & 0 \\ 0 & 0 & 0 & 1 & 1 & 0 \\ 0 & 0 & 0 & 0 & 1 & 1 \\ 0 & 0 & 0 & 0 & 0 & 1 \end{array} \right]$	$\left[\begin{array}{c c} 1 & 0 \\ 0 & 0 \\ 0 & 0 \\ 0 & 1 \end{array} \right]$

Table 3. Tableaux projections T_{123} and T_4 before and after $CNOT_{3,4}$ is applied to $|\phi\rangle$. The action of $CNOT_{3,4}$ increases the rank of T_{123} , which yields a violation of $MMI_{\{1,2,3\}}$, the MMI instance involving the tripartite subsystem $\{1, 2, 3\}$. The rank of T_4 also increases consistently with the equality of entanglement entropies for complementary subsystems, given by $T_A - T_{\bar{A}} = |A| - |\bar{A}|$.

Table 3 reveals that $CNOT_{3,4}$ introduces a fourth nonzero, linearly independent row in the projected tableau T_{123} , thereby increasing its rank from 3 to 4. Notably, this same $CNOT_{3,4}$ action on $|\phi\rangle$ preserves the T_{123} column substructure that determines the first six entries of the rank vectors in Table 2, with R_{123} the only component affected by this gate.

Before the $CNOT_{3,4}$ gate is applied, all X columns in T_{123} are linearly dependent, while all Z columns are pairwise linearly independent. Consequently, every length-one subsystem of $\{123\}$ is described by a tableau containing exactly one X column and one Z column, therefore guaranteeing a rank of 2. Similarly, each length-two subsystem contains two X and two Z columns, giving a rank of 3. Preserving the X and Z column dependencies, while increasing the rank of T_{123} , generates the $MMI_{\{1,2,3\}}$ equality breaking that leads to violation. This analysis demonstrates that MMI violation in stabilizer states can be understood from the transformations of row/column spaces of tableau projections. In the next section we show how representing this construction in a graph-state formalism enables a compact and explicit qualification for MMI violation in stabilizer states.

3.2 Entanglement Entropies From the Adjacency Matrices

We now translate the tableau rank calculation from the previous section into a graph-theoretic formalism. Recall that graph states, while constituting a proper subset of stabilizer states, realize all possible stabilizer entropy vectors. For an undirected simple graph G , which realizes the graph state $|G\rangle$, let Γ_G indicate the adjacency matrix for G . For any subsystem $\mathcal{L} \subseteq |G\rangle$, Eq. (2.20) defines the local information submatrix $\Gamma^{\mathcal{L}}$, constructed from Γ . The submatrix $\Gamma^{\mathcal{L}}$ contains all information

needed to compute the entanglement entropy of \mathcal{L} . Moreover, $\Gamma^{\mathcal{L}}$ characterizes the connectivity between sets of vertices in the associated graph G , and simplifies the requisite MMI calculations as we will demonstrate in Sections 4.1 and 4.2.

We illustrate the calculation of entanglement entropy from a graph's adjacency matrix using the graph state $|K_4\rangle$, representable by the 4-vertex star graph K_4 shown in Figure 2 and constructable as

$$|K_4\rangle = CZ_{1,4}CZ_{1,3}CZ_{1,2}|+\rangle^{\otimes 4}. \quad (3.8)$$

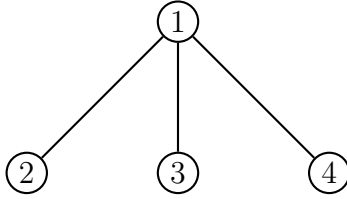


Figure 2. Graph Representation for $|K_4\rangle$, a state LC equivalent to $|GHZ\rangle_4$, which violates all 3-party instances of MMI.

The graph state $|K_4\rangle$ is LC equivalent to the 4-qubit GHZ state $|GHZ\rangle_4$ through

$$|GHZ\rangle = H_4H_3H_2|K_4\rangle. \quad (3.9)$$

Following Figure 2, the K_4 adjacency matrix only contains non-zero elements in the first row and column, and is written

$$\Gamma = \begin{bmatrix} 0 & 1 & 1 & 1 \\ 1 & 0 & 0 & 0 \\ 1 & 0 & 0 & 0 \\ 1 & 0 & 0 & 0 \end{bmatrix}. \quad (3.10)$$

We evaluate $MMI_{\{1,3,4\}}$, which corresponds to the MMI instance in Eq. (2.5) on the disjoint subsystems $C = \{1\}$, $I = \{3\}$, and $J = \{4\}$. The local information submatrix of $\mathcal{L} = \{1, 3, 4\}$ is

$$\Gamma^{\mathcal{L}} = \begin{bmatrix} 0 & 1 & 1 & 1 \\ 1 & 0 & 0 & 0 \\ 1 & 0 & 0 & 0 \end{bmatrix}. \quad (3.11)$$

For a subsystem A , involved in an MMI calculation, the local information submatrix Γ^A is easily obtained from $\Gamma^{\mathcal{L}}$ by selecting the rows indexed by elements in A and the columns indexed by elements in its complement \bar{A} . Figure 3 illustrates this selection process. Following Eq. (2.19), the entanglement entropy of A is computed as the rank of Γ^A , over \mathbb{Z}_2 .

$$\begin{array}{cc}
\Gamma^{\{1\}} & \Gamma^{\{1,3\}} \\
\left[\begin{array}{|c|c|c|c|} \hline 0 & 1 & 1 & 1 \\ \hline 1 & 0 & 0 & 0 \\ \hline 1 & 0 & 0 & 0 \\ \hline \end{array} \right] & \left[\begin{array}{|c|c|c|c|} \hline 0 & 1 & 1 & 1 \\ \hline 1 & 0 & 0 & 0 \\ \hline 1 & 0 & 0 & 0 \\ \hline \end{array} \right] \\
\\
\Gamma^{\{3\}} & \Gamma^{\{1,4\}} \\
\left[\begin{array}{|c|c|c|c|} \hline 0 & 1 & 1 & 1 \\ \hline 1 & 0 & 0 & 0 \\ \hline 1 & 0 & 0 & 0 \\ \hline \end{array} \right] & \left[\begin{array}{|c|c|c|c|} \hline 0 & 1 & 1 & 1 \\ \hline 1 & 0 & 0 & 0 \\ \hline 1 & 0 & 0 & 0 \\ \hline \end{array} \right] \\
\\
\Gamma^{\{4\}} & \Gamma^{\{3,4\}} \\
\left[\begin{array}{|c|c|c|c|} \hline 0 & 1 & 1 & 1 \\ \hline 1 & 0 & 0 & 0 \\ \hline 1 & 0 & 0 & 0 \\ \hline \end{array} \right] & \left[\begin{array}{|c|c|c|c|} \hline 0 & 1 & 1 & 1 \\ \hline 1 & 0 & 0 & 0 \\ \hline 1 & 0 & 0 & 0 \\ \hline \end{array} \right] \\
\\
\Gamma^{\{1,3,4\}} \\
\left[\begin{array}{|c|c|c|c|} \hline 0 & 1 & 1 & 1 \\ \hline 1 & 0 & 0 & 0 \\ \hline 1 & 0 & 0 & 0 \\ \hline \end{array} \right]
\end{array}$$

Figure 3. For each distinct bipartition $\{A, \bar{A}\}$ of $\mathcal{L} = \{1, 3, 4\}$, rows indexed by vertices in A and columns indexed by vertices in \bar{A} are outlined; their intersection defines Γ^A , which is shaded. S_A is independent of intra-subsystem adjacencies within the partition $\{A, \bar{A}\}$, that is, of the adjacencies within A itself and within \bar{A} itself. Observe that each Γ^A shown has rank 1.

Each matrix in Figure 3 has rank 1, and thus the entanglement entropy of each subsystem is likewise 1. As demonstrated in Section 3.1, a 4-qubit entropy vector with each component 1 will violate all 3-party instances of $MMI_{\{1,3,4\}}$.

Connecting a fifth vertex to any leg of the 4-star graph representing $|K_4\rangle$ produces a new graph state $|K_4^{1,1,2}\rangle$, which is not LC equivalent to a GHZ state. Nonetheless, the state $|K_4^{1,1,2}\rangle$ still violates MMI due to the GHZ -type entanglement present on four of its vertices. For example, let $K_4^{1,1,2}$ be the graph obtained by connecting a fifth vertex to vertex 4 of the K_4 graph in Figure 2. The state $|K_4^{1,1,2}\rangle$ can be constructed as $CZ_{4,5}(|K_4\rangle \otimes |+\rangle)$, and its associated graph $K_4^{1,1,2}$ is given in Figure 4.

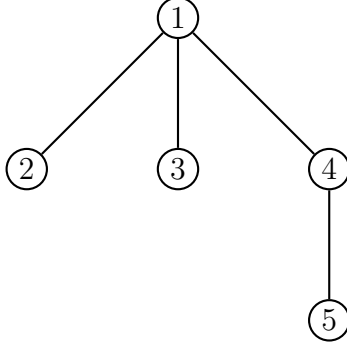


Figure 4. Graph Representation for $|K_4^{1,1,2}\rangle = CZ_{4,5}(|K_4\rangle \otimes |+\rangle)$, with a four-star K_4 induced by vertices $\{1, 2, 3, 4\}$. While $|K_4^{1,1,2}\rangle$ is not a GHZ state, it nevertheless fails $MMI_{\{1,3,4,5\}}$ due to its star topology.

Following from Figure 4, the adjacency matrix for $K_4^{1,1,2}$ is given by

$$\Gamma = \begin{bmatrix} 0 & 1 & 1 & 1 & 0 \\ 1 & 0 & 0 & 0 & 0 \\ 1 & 0 & 0 & 0 & 0 \\ 1 & 0 & 0 & 0 & 1 \\ 0 & 0 & 0 & 1 & 0 \end{bmatrix}. \quad (3.12)$$

As before, we evaluate $MMI_{\{1,3,4,5\}}$ using the local information submatrix for $\mathcal{L} = \{1, 3, 4, 5\}$, written

$$\Gamma^{\mathcal{L}} = \begin{bmatrix} 0 & 1 & 1 & 1 & 0 \\ 1 & 0 & 0 & 0 & 0 \\ 1 & 0 & 0 & 0 & 1 \\ 0 & 0 & 0 & 1 & 0 \end{bmatrix}. \quad (3.13)$$

Figure 5 shows a breakdown of $\Gamma^{\mathcal{L}}$ into blocks, with the respective shared information elements highlighted.

	C	I	J	K
	CC	CI	CJ	CK
C	0	1	1	0
	IC	II	IJ	IK
I	1	0	0	0
	JC	JI	JJ	JK
J	1	0	0	1
	IC	JI	JJ	JK
	0	0	1	0

Figure 5. Local information submatrix $\Gamma^{\mathcal{L}}$, for $\mathcal{L} = \{1, 3, 4, 5\}$ in $|K_4^{1,1,2}\rangle$, given in block matrix form. The state $|K_4^{1,1,2}\rangle$ is partitioned such that $C \sqcup I \sqcup J \sqcup K = \{1, 2, 3, 4, 5\}$, and shared information elements are colored. Notice that S_A for $A \subseteq \mathcal{L}$ is independent of the self adjacency blocks CC , II , and JJ , which are shaded gray.

Figure 6 gives every local information submatrix needed to evaluate $MMI_{\{1,3,4,5\}}$:

$$\begin{aligned}
& \text{rank}(\Gamma^{\{1\}}) + \text{rank}(\Gamma^{\{3\}}) + \text{rank}(\Gamma^{\{4,5\}}) + \text{rank}(\Gamma^{\{1,3,4,5\}}) \\
& \stackrel{?}{\leq} \text{rank}(\Gamma^{\{1,3\}}) + \text{rank}(\Gamma^{\{1,4,5\}}) + \text{rank}(\Gamma^{\{3,4,5\}}),
\end{aligned} \tag{3.14}$$

where all ranks are taken over \mathbb{Z}_2 , as the entanglement from adjacency matrix formula Eq. (2.19) requires. Inspection of Figure 6 reveals that each term in Eq. (3.14) has rank 1, giving an entanglement entropy of 1, thereby yielding a violation of $MMI_{\{1,3,4,5\}}$ for $|K_4^{1,1,2}\rangle$.

$\Gamma^{\{1\}} = \begin{bmatrix} \boxed{0} & \boxed{1} & \boxed{1} & \boxed{1} & \boxed{0} \\ 1 & 0 & 0 & 0 & 0 \\ 1 & 0 & 0 & 0 & 1 \\ 0 & 0 & 0 & 1 & 0 \end{bmatrix}$	$\Gamma^{\{1,3\}} = \begin{bmatrix} \boxed{0} & \boxed{1} & \boxed{1} & \boxed{1} & \boxed{0} \\ 1 & \boxed{0} & \boxed{0} & \boxed{0} & \boxed{0} \\ 1 & 0 & 0 & 0 & 1 \\ 0 & 0 & 0 & 1 & 0 \end{bmatrix}$
$\Gamma^{\{3\}} = \begin{bmatrix} \boxed{0} & \boxed{1} & \boxed{1} & \boxed{1} & \boxed{0} \\ 1 & \boxed{0} & \boxed{0} & \boxed{0} & \boxed{0} \\ 1 & 0 & 0 & 0 & 1 \\ 0 & 0 & 0 & 1 & 0 \end{bmatrix}$	$\Gamma^{\{1,4,5\}} = \begin{bmatrix} \boxed{0} & \boxed{1} & \boxed{1} & \boxed{1} & \boxed{0} \\ 1 & \boxed{0} & \boxed{0} & \boxed{0} & \boxed{0} \\ 1 & 0 & 0 & 0 & 1 \\ 0 & \boxed{0} & \boxed{0} & \boxed{1} & \boxed{0} \end{bmatrix}$

$$\begin{array}{c}
\Gamma\{4,5\} \\
\left[\begin{array}{|c|c|c|c|c|} \hline 0 & 1 & 1 & 1 & 0 \\ \hline 1 & 0 & 0 & 0 & 0 \\ \hline 1 & 0 & 0 & 0 & 1 \\ \hline 0 & 0 & 0 & 1 & 0 \\ \hline \end{array} \right]
\end{array}
\qquad
\begin{array}{c}
\Gamma\{3,4,5\} \\
\left[\begin{array}{|c|c|c|c|c|} \hline 0 & 1 & 1 & 1 & 0 \\ \hline 1 & 0 & 0 & 0 & 0 \\ \hline 1 & 0 & 0 & 0 & 1 \\ \hline 0 & 0 & 0 & 1 & 0 \\ \hline \end{array} \right]
\end{array}$$

$$\begin{array}{c}
\Gamma\{1,3,4,5\} \\
\left[\begin{array}{|c|c|c|c|c|} \hline 0 & 1 & 1 & 1 & 0 \\ \hline 1 & 0 & 0 & 0 & 0 \\ \hline 1 & 0 & 0 & 0 & 1 \\ \hline 0 & 0 & 0 & 1 & 0 \\ \hline \end{array} \right]
\end{array}$$

Figure 6. For each bipartition $\{A, \bar{A}\}$ of $\mathcal{L} = \{1, 3, 4, 5\}$, rows indexed by A and columns indexed by \bar{A} are outlined. The intersection of these rows and columns defines Γ^A , which is shaded. S_A is independent of intra-subsystem adjacencies within the partition $\{A, \bar{A}\}$, that is, of the adjacencies within A itself and within \bar{A} itself. For state $|K_4^{1,1,2}\rangle$, every Γ^A has rank 1, and therefore $|K_4^{1,1,2}\rangle$ fails $MMI_{\{1,3,4,5\}}$.

In this section we showed how the MMI inequalities can be reformulated in terms of tableau submatrix ranks, and demonstrated how entangling operations, e.g. a *CNOT* gate, alter submatrix rank to induce MMI violations. Tracking the row and column space transformations of tableau projections, we identified the mechanism that leads to MMI violation in graph states that are *LC* equivalent to 4-qubit GHZ states, and other graph states with an equivalent entanglement structure. We extended this construction to a graph-theoretic setting, where the condition for MMI violation manifests as a forbidden-subgraph structure that embodies *GHZ*-type entanglement. Evaluating MMI using the ranks of graph state adjacency matrices, we explicitly showed how MMI violation is compactly diagnosed by the local information submatrices of subsystems involved in the inequalities. In the next section we lay out necessary conditions for a family of graph states to violate particular MMI instances, and discuss the physical interpretations for these requirements.

4 Conditions for MMI Violation in Graph States

In this section, we characterize the structural conditions for violation of specific MMI families in graph states. We analyze the relationship between graph connectivity and the entanglement entropy between disjoint graph state subsystems, identifying the explicit conditions that guarantee failure of these specific MMI instances. We

first consider a specific class of star-like graphs G , featuring a single central vertex c connected to disjoint and disconnected subgraphs, and derive the necessary and sufficient conditions under which such graphs violate a family of MMI instances MMI_{cIJ} . We then extend this framework to consider generalized star graphs \mathcal{G} , possessing a multi-vertex center C , and algebraically relate failure of the analogous MMI family MMI_{CIJ} to specific intersection and distributivity properties of adjacency matrix column spaces. We highlight the physical implications of the violation of these specific MMI instances in graph states, and present several observations of significance.

4.1 An MMI-Violating Graph

We now derive the necessary conditions for a family of graph states to violate the MMI instances MMI_{cIJ} , defined in Eq. (4.2).

Let $G = (V, E)$ be a graph on n vertices that consists of a central vertex c connected to $k \geq 3$ nonempty subgraphs,

$$G^1, G^2, \dots, G^k, \quad (4.1)$$

which are vertex-disjoint and mutually³ disconnected, and where each $G^p = (V^p, E^p)$ for $p = 1, 2, \dots, k$. For any pair of indices $p, q \in \{1, 2, \dots, k\}$, such that $p \neq q$, the graph G satisfies the following conditions:

- (1) If $v \in V^p$, then $v \notin V^q$ (subgraph disjointness),
- (2) The set $\{\{c\}, V^1, V^2, \dots, V^k\}$ defines a partition of V (graph partitioning).
- (3) For every $v \in V^p$ and $w \in V^q$, we have $(v, w) \notin E$ (inter-subgraph disconnectedness).
- (4) There exists at least one $v \in V^p$ such that $(v, c) \in E$ (subgraph anchoring),

When considering a particular instance of MMI we will fix a partition of the vertices $V \setminus c$ into three subsets I, J and $K := V \setminus \{c, I, J\}$, where I, J, K are each unions of the vertex sets V^p . A schematic diagram for such a graph G is presented in Figure 7.

³Multiple edges may exist between the central vertex c and each disjoint subgraph G^p .

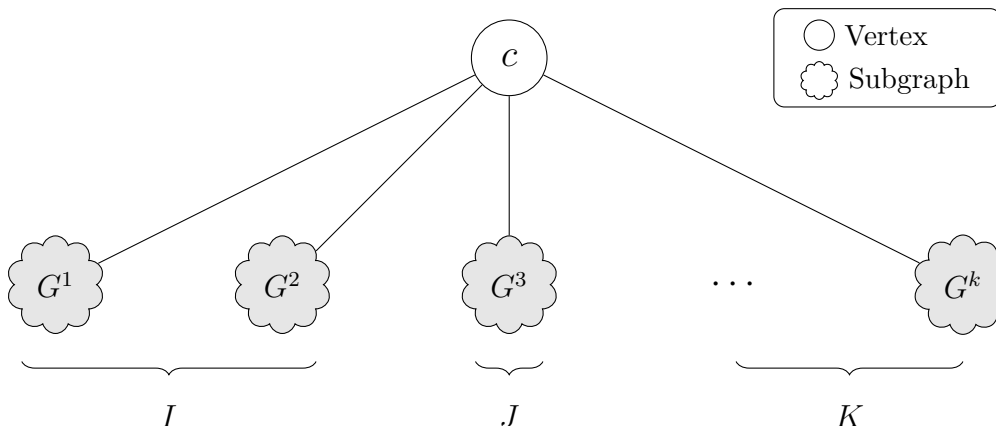


Figure 7. Generalized star graph G which satisfies the conditions of subgraph disjointness, graph partitioning, subgraph anchoring, and inter-subgraph disconnectedness. The subsystems $\{c\}$, I , J , and K give a valid partition that defines MMI_{cIJ} , as in Eq. (4.2), where any path between the subsystems I , J and K must include the central vertex c . Any graph state represented by a graph of type G will have an entropy vector that violates MMI_{cIJ} .

Having defined the class of graphs G , which satisfy the properties of subgraph disjointness, graph partitioning, subgraph anchoring, and inter-subgraph disconnectedness, we now prove that any graph state $|G\rangle$ violates⁴ MMI_{cIJ} .

Proposition 1. *Every graph state $|G\rangle$, represented by a graph G which admits the properties of subgraph disjointness, graph partitioning, subgraph anchoring, and inter-subgraph disconnectedness, has an entropy vector that violates every MMI_{cIJ} , which is of the form*

$$S_{cI} + S_{cJ} + S_{IJ} \geq S_c + S_I + S_J + S_{cIJ}, \quad (4.2)$$

where c denotes the subsystem containing the central vertex, and $I, J \subset V \setminus c$ such that $I \cap J = \emptyset$, $\overline{c \sqcup I \sqcup J} \neq \emptyset$, and any path between I, J and K must include c .

Proof. We prove the proposition by showing that each term in MMI_{cIJ} , as in Eq. (4.2) has value 1. This result follows from the fact that the adjacency submatrices, relevant to the MMI_{cIJ} entries in Eq. (4.2), only have nonzero entries along a single row or column.

For a graph state $|G\rangle$, the selection of disjoint subsystems $c, I, J \subseteq |G\rangle$ induce the vertex partition $V = c \sqcup I \sqcup J \sqcup K$ on G . Let $\mathcal{L} = c \sqcup I \sqcup J$ which, after a vertex

⁴We emphasize that the condition $k \geq 3$, in Eq. (4.1), is important since states GHZ_n , for $n \leq 3$, will satisfy MMI_{cIJ} as the adjacency submatrix ranks can produce entropies of 0.

permutation, admits the local information submatrix $\Gamma^{\mathcal{L}}$ as

$$\Gamma^{\mathcal{L}} = \begin{bmatrix} 0 & cI & cJ & cK \\ (cI)^T & II & IJ & IK \\ (cJ)^T & (IJ)^T & JJ & JK \end{bmatrix}. \quad (4.3)$$

In this representation, each block of $\Gamma^{\mathcal{L}}$ contains adjacencies between the two sub-systems which label that block, i.e. each entry of $\Gamma^{\mathcal{L}}$ is a block matrix $(\Gamma)_{u,v}$ with $u, v \in \{c, I, J, K\}$.

Second, the condition of inter-subgraph disconnectedness (3) requires that the block structure of $\Gamma^{\mathcal{L}}$ obeys the constraints

$$\begin{aligned} IJ &= \mathbf{0}_{IJ}, \\ IK &= \mathbf{0}_{IK}, \\ JK &= \mathbf{0}_{JK}, \end{aligned} \quad (4.4)$$

where $\mathbf{0}_{IJ}$ denotes the zero matrix of size $|I| \times |J|$. Omitting the dimensionality of the block-zero matrices, for conciseness and since each is fixed by its adjacent blocks, allows $\Gamma^{\mathcal{L}}$ in Eq. (4.3) to be rewritten as

$$\Gamma^{\mathcal{L}} = \begin{bmatrix} 0 & cI & cJ & cK \\ (cI)^T & II & \mathbf{0} & \mathbf{0} \\ (cJ)^T & \mathbf{0} & JJ & \mathbf{0} \end{bmatrix}. \quad (4.5)$$

For each subset $A \subseteq \mathcal{L}$, the local information submatrix Γ^A can be read directly from $\Gamma^{\mathcal{L}}$ using the definition of these matrices provided in Eq. (2.20). The rank of each Γ^A determines the entanglement entropy S_A , as given by Eq. (2.19). Therefore all terms needed to evaluate MMI_{cIJ} are computed as

$$\begin{aligned} S_c &= \text{rank} \left(\begin{bmatrix} cI & cJ & cK \end{bmatrix} \right) & S_{cI} &= \text{rank} \left(\begin{bmatrix} cJ & cK \end{bmatrix} \right) \\ S_I &= \text{rank} (cI) & S_{cJ} &= \text{rank} \left(\begin{bmatrix} cI & cK \end{bmatrix} \right) \\ S_J &= \text{rank} (cJ) & S_{IJ} &= \text{rank} \left(\begin{bmatrix} cI & cJ \end{bmatrix} \right) \end{aligned} \quad (4.6)$$

$$S_{cIJ} = \text{rank} (cK)$$

Each entropy in Eq. (4.6) corresponds to the rank of a single-row matrix, which can take value 0 or 1, with a value of 1 occurring if and only if the matrix contains a non-zero entry. However, the subgraph anchoring condition (4) guarantees that cI , cJ , and cK each contain at least one nonzero entry. Consequently, the rank of each matrix in Eq. (4.6) is 1, and thus each entropy $S_A = 1$. Therefore any graph state $|G\rangle$ will have an entropy vector that fails MMI_{cIJ} . \square

In the above section, we derived the structural conditions under which a graph state belonging to the family G will violate the MMI_{cIJ} as in Eq. (4.2). We demonstrated that any graph G , composed of a single central vertex connected to mutually disjoint and disconnected subgraphs, always possesses an entropy vector that fails MMI_{cIJ} . For each subsystem of $|G\rangle$ involved in the MMI_{cIJ} evaluation, we showed how the block structure of the adjacency submatrix yields an entanglement entropy of 1, leading to a guaranteed violation of this MMI instance. Accordingly, we established that MMI_{cIJ} violation inevitably occurs in graph states with a star topology, as in Figure 7, satisfying the conditions of subgraph disjointness (1), graph partition (2), subgraph disconnectedness (3), and subgraph anchoring (4). We now generalize our proof to include graphs where the central vertex c is promoted to a multi-vertex subgraph.

4.2 Characterization of MMI Family Violation in a Larger Family of Graph States

We now extend the class of graphs G , introduced in Section 4.1, by generalizing the single central vertex c to a multi-vertex subgraph C , as depicted in Figure 8. In these generalized star graphs, denoted \mathcal{G} , we identify the failure conditions for the MMI instance MMI_{CIJ} . We show that subgraph anchoring (4), is no longer sufficient to guarantee failure of MMI_{CIJ} , and detail additional requirements for violation.

We define $\mathcal{G} = (V, E)$ as a graph on n vertices, with a central subgraph C consisting of vertices $\{c_1, c_2, \dots, c_m\}$. The subgraph C is connected to k non-empty subgraphs,

$$\mathcal{G}^1, \mathcal{G}^2, \dots, \mathcal{G}^k, \quad (4.7)$$

that are both vertex-disjoint and mutually disconnected, and where each $\mathcal{G}^p = (V^p, E^p)$ for $p = 1, 2, \dots, k$. As before, for any pair of indices $p, q \in \{1, 2, \dots, k\}$ such that $p \neq q$, the graph \mathcal{G} satisfies the following conditions:

- (1) If $v \in V^p$, then $v \notin V^q$ (subgraph disjointness).
- (2) The set $\{C, V^1, V^2, \dots, V^k\}$ defines a partition of V (graph partitioning).
- (3) For every $v \in V^p$ and $w \in V^q$, we have $(v, w) \notin E$ (inter-subgraph disconnectedness).

These conditions do not capture the generalization of subgraph anchoring which requires a more detailed discussion as below (see Observation 4). A schematic representation for graphs of the form \mathcal{G} is given in Figure 8.

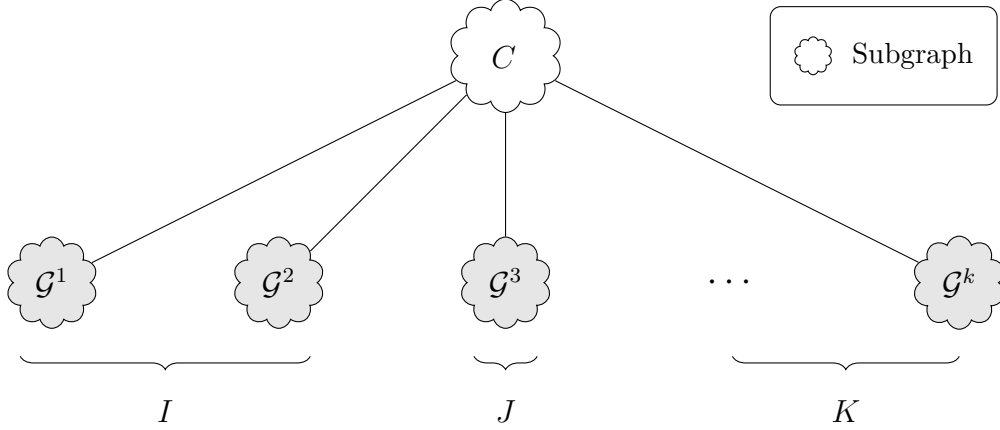


Figure 8. Graph \mathcal{G} , the generalization of G in Figure 7, with the central vertex c promoted to the subgraph C . Every \mathcal{G} satisfies the subgraph disjointness, graph partition, and inter-subgraph disconnectedness conditions, but not subgraph anchoring. Subsystems C , I , and J partition the vertices of \mathcal{G} , defining MMI_{CIJ} in Eq. (4.8), and every path between I , J and K must only include vertices in C . Not every $|\mathcal{G}\rangle$ violates MMI_{CIJ} , as shown in Table 6.

Given graphs of the form \mathcal{G} , we now seek to determine under what conditions the state $|\mathcal{G}\rangle$ fails MMI_{CIJ} ,

$$S_{CI} + S_{CJ} + S_{IJ} \geq S_C + S_I + S_J + S_{CIJ}, \quad (4.8)$$

where I and J are defined as in Section 4.1 with $I, J \subset V \setminus C$ such that $I \cap J = \emptyset$ and $\overline{C \sqcup I \sqcup J} \neq \emptyset$. As before, subgraph disjointness (2) and graph partitioning (2) guarantee that the choice of C , I , and J defines the partition $V = C \sqcup I \sqcup J \sqcup K$. We set $\mathcal{L} = C \sqcup I \sqcup J$, and express the local information submatrix $\Gamma^{\mathcal{L}}$ in block form

$$\Gamma^{\mathcal{L}} = \begin{bmatrix} CC & CI & CJ & CK \\ (CI)^T & II & \mathbf{0} & \mathbf{0} \\ (CJ)^T & \mathbf{0} & JJ & \mathbf{0} \end{bmatrix}, \quad (4.9)$$

immediately imposing inter-subgraph disconnectedness (3). The first row of $\Gamma^{\mathcal{L}}$ in Eq. (4.9) is now a row of block matrices, instead of a row of numbers as was the case for G .

We can reformulate MMI_{CIJ} in terms of the dimensions of intersections and sums of block matrix column spaces, as detailed in Appendix A.1. Applying this rewriting, MMI_{CIJ} becomes

$$\begin{aligned} & \dim \{ \text{Col}(CI) \cap \text{Col}(CK) \} + \dim \{ \text{Col}(CJ) \cap \text{Col}(CK) \} \\ & \leq \dim \{ (\text{Col}(CI) + \text{Col}(CJ)) \cap \text{Col}(CK) \}. \end{aligned} \quad (4.10)$$

In Eq. (4.10) $\text{Col}(M)$ denotes the column space of the matrix M , i.e. the linear subspace spanned by the columns of M . Thereby $\dim\{\text{Col}(CI) \cap \text{Col}(CK)\}$ is the dimension of the subspace formed by the intersection of the column space of block matrix CI and the column space of CK . Importantly, addition inside of the dimension evaluation in Eq. (4.10) corresponds to subspace addition, which is not simply the union of two subspaces, but instead the set of all possible sums of elements in both subspaces.

For compactness, let $W_I = \text{Col}(CI)$, $W_J = \text{Col}(CJ)$, and $W_K = \text{Col}(CK)$. Using Eqs. (A.5) and (A.6) from Appendix A.2, which detail the arithmetic for the dimension of sums of subspaces and the property of subspace inclusion, respectively, we derive the following inequality for column spaces:

$$\dim\{W_I \cap W_K\} + \dim\{W_J \cap W_K\} - \dim\{W_I \cap W_J \cap W_K\} \leq \dim\{(W_I + W_J) \cap W_K\}. \quad (4.11)$$

Eq. (4.11) differs from the MMI_{CIJ} reformulation in Eq. (4.10) only by the subtraction of term $\dim\{W_I \cap W_J \cap W_K\}$. Another important property that enables our analysis of MMI is subspace distributivity. The subspaces W_I , W_J and W_K are said to be distributive⁵ linear subspaces of $\mathbb{Z}_2^{|C|}$ if

$$W_I \cap W_K + W_J \cap W_K = (W_I + W_J) \cap W_K. \quad (4.12)$$

Using Eqs. (4.11) and (4.12) we now classify distinct realizations of \mathcal{G} according to whether W_I , W_J , and W_K have a trivial intersection and are distributive. For the states $|\mathcal{G}\rangle$ belonging to each class, we deduce directly from Eq. (4.11) whether they strictly satisfy, saturate, or fail the specified MMI_{CIJ} in Eq. (4.8). A proof for each case is provided in Appendix A.2. Table 6 provides a summary of our classification.

Case	Distributive	Nontrivial Intersection	MMI_{CIJ} Evaluation
1	No	No	Satisfies
2	Yes	No	Saturates
3	Yes	Yes	Fails
4	No	Yes	Undetermined

Table 6. Evaluation criteria for MMI_{CIJ} , in Eq. (4.8), for graph states $|\mathcal{G}\rangle$ based on the intersection $W_I \cap W_J \cap W_K$ and the distributivity of $W_I = \text{Col}(CI)$, $W_J = \text{Col}(CJ)$, and $W_K = \text{Col}(CK)$ defined in Eq. (4.12).

Tables 7 and 8 provide explicit \mathcal{G} realizations of every case in Table 6.

⁵If Eq. (4.12) is true, then distributivity also holds for every permutation of $\{W_I, W_J, W_K\}$.

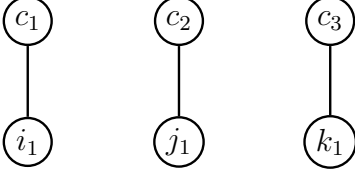
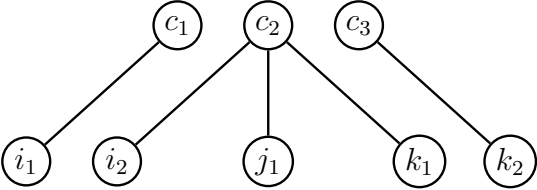
Case	\mathcal{G} Representative
1	 <p>Non-distributive; trivial intersection</p>
2	 <p>Distributive; trivial intersection</p>
3	 <p>Distributive; non-trivial intersection</p>

Table 7. \mathcal{G} instances illustrating Cases 1–3 of the MMI_{CIJ} (4.8) categorization for $|\mathcal{G}\rangle$ states, as listed in Table 6. Each example depicts the subspace structure defined by the column spaces of CI , CJ , and CK , associated with the tripartite subsystem $\{C, I, J\}$. Within the partition $\{C, I, J, K\}$, every vertex in each graph belongs to the subsystem that labels it (i.e., $c_p \in C$, $i_q \in I$, and $j_m \in J$ for all $c_p, i_q, j_m \in V$). Notice that the subgraph induced by C is not required to be connected.

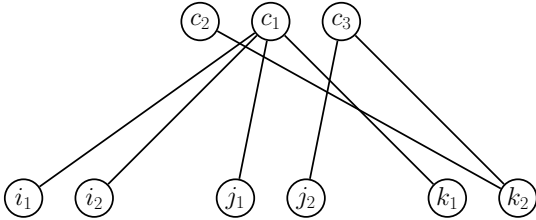
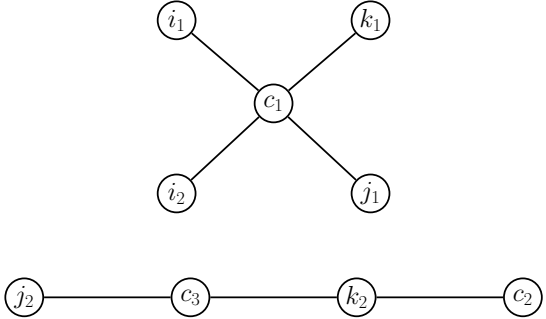
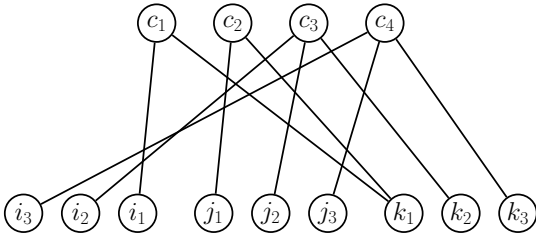
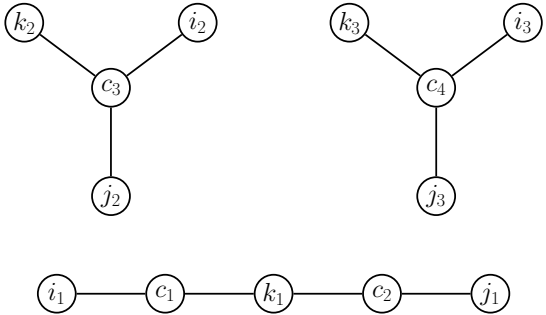
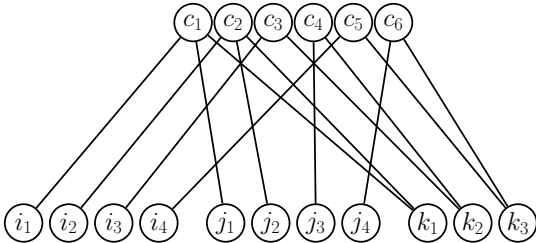
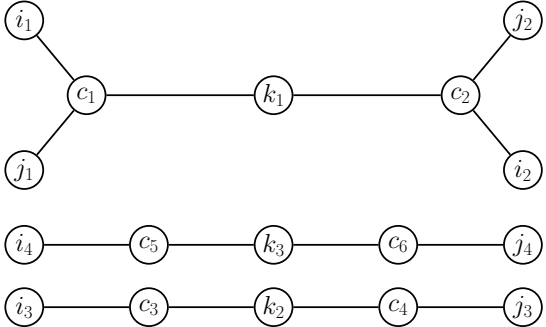
\mathcal{G} Representative	Isomorphic Form
Saturates	
	
Fails	
	
Satisfies	
	

Table 8. \mathcal{G} representatives illustrating every MMI_{CIJ} (4.8) outcome belonging to Case 4 (undetermined) of the categorization shown in Table 6. Each representative is accompanied by an isomorphic form that makes its disconnected structure explicit. Every example exhibits non-distributive and nontrivially intersecting column spaces of CI , CJ , and CK (see Table 10 in Appendix A.2 for additional details), all associated with the tripartite subsystem $\{C, I, J\}$. Within the partition $\{C, I, J, K\}$, every vertex in each graph belongs to the subsystem that labels it (i.e., $c_p \in C$, $i_q \in I$, and $j_m \in J$ for all $c_p, i_q, j_m \in V$). The outcome of MMI_{CIJ} (4.8) for $|\mathcal{G}|$ labels each \mathcal{G} .

The results of Table 6 can be summarized by the following observations, each referring to MMI_{CIJ} in Eq. (4.8).

Observation 1. *If $\text{Col}(CI)$, $\text{Col}(CJ)$, and $\text{Col}(CK)$ are distributive, then $|\mathcal{G}\rangle$ cannot strictly satisfy MMI_{CIJ} (4.8).*

Observation 2. *The condition $\text{Col}(CI) \cap \text{Col}(CJ) \cap \text{Col}(CK) \neq \emptyset$ is necessary for $|\mathcal{G}\rangle$ to fail MMI_{CIJ} (4.8).*

Observation 3. *If $\text{Col}(CI)$, $\text{Col}(CJ)$, and $\text{Col}(CK)$ are distributive and have a nontrivial intersection, then $|\mathcal{G}\rangle$ fails MMI_{CIJ} (4.8).*

For consistency, we further verify that any graph of the class \mathcal{G} that violates MMI_{CIJ} (4.8) is of type G when its central subgraph C consists of a single vertex, as in Section 4.1. When subgraph C contains only a single vertex c , then W_I , W_J , and W_K are subspaces of the one-dimensional vector space \mathbb{Z}_2 . By Observation 2, these subspaces must have a nontrivial intersection for $|\mathcal{G}\rangle$ in order to fail MMI_{CIJ} (4.8). Since the only subspaces of \mathbb{Z}_2 are

$$\left\{ [0] \right\} \text{ and } \left\{ [0], [1] \right\}, \quad (4.13)$$

the condition for W_I , W_J , and W_K to share a nontrivial intersection is satisfied only when

$$W_1 = W_2 = W_3 = \left\{ [0], [1] \right\}, \quad (4.14)$$

which is precisely the subgraph anchoring condition (4) from Section 4.1. Therefore, any graph \mathcal{G} that falls into Case 3 of Table 6 reduces to a graph of the form G when $|C| = 1$.

More generally, the evaluation of MMI_{CIJ} (4.8) for $|\mathcal{G}\rangle$ trivially reduces to Case 3 in Table 6 when $W_I = W_J = W_K$, failing MMI_{CIJ} by all entropies being equal (see A.1). Since this particular MMI_{CIJ} violation is identical to the violation of MMI_{CIJ} (4.2) exhibited by states $|G\rangle$, we define the following generalization of $|G\rangle$ that is guaranteed to always fail MMI_{CIJ} (4.8).

Observation 4. *Define G' to have the following properties:*

- (1) Is a generalized star \mathcal{G} under the partition $\{C, I, J, K\}$.
- (2) The $\{C, I, J, K\}$ partition obeys

$$\text{Col}(CI) = \text{Col}(CJ) = \text{Col}(CK) \quad (\text{generalized subgraph anchoring}).$$

Then, the state $|G'\rangle$ will always fail MMI_{CIJ} (4.8) as a result of

$$S_A = \text{rank}(CI) = \text{rank}(CJ) = \text{rank}(CK), \text{ for every } A \subset CIJ. \quad (4.15)$$

The characteristic MMI_{CIJ} (4.8) failure exhibited by $|G'\rangle$ in Observation 4 can be interpreted as a generalized GHZ -type MMI violation. Furthermore, for a state $|\mathcal{G}\rangle$, the column spaces of CI , CJ , and CK are trivially distributive whenever two or more subspaces are equal, preventing the state from strictly satisfying MMI_{CIJ} (4.8) by Observation 1.

In this section, we extended the central-vertex star graphs G introduced in Section 4.1 to a broader class of graphs \mathcal{G} , in which the central vertex c is replaced by a multi-vertex subgraph C . We derived the conditions under which the graph states $|\mathcal{G}\rangle$ violate MMI_{CIJ} (4.8), demonstrating that subgraph anchoring is no longer a sufficient condition to guarantee violation. Instead we showed how the relationship between column space distributivity and intersection, in the adjacency submatrices for parties involved in MMI_{CIJ} (4.8), determines satisfaction, saturation, and failure of the inequalities. We provided a classification of MMI_{CIJ} (4.8) evaluation for all realizations of \mathcal{G} , summarized in Table 6. Finally, we verified that graphs \mathcal{G} reduce to the form G when the central subgraph C consists of a single vertex, and introduced a generalization of G that is guaranteed to always fail MMI_{CIJ} (4.8) by containing a GHZ -type subgraph. In the next section we provide a physical interpretation for our MMI_{CIJ} (4.8) failure conditions in the context of quantum circuits.

4.3 A Physical Interpretation of the MMI_{CIJ} Violation Conditions

In Section 4.2 we established conditions to determine if a state whose graph representation is LC equivalent to a graph of type \mathcal{G} satisfies, saturates, or violates MMI_{CIJ} (4.8). Our analysis relied on an algebraic reformulation of the MMI_{CIJ} (4.8) inequality into a relation between the column spaces of adjacency matrix blocks CI , CJ , and CK , for $|\mathcal{G}\rangle$ subsystems C , I , J , and K . We now give a physical interpretation for these algebraic conditions by moving from a vector space formalism into the language of quantum circuits.

4.3.1 From Column Spaces to Reachable Circuits

Following Eq. (2.17), an n -qubit graph state $|G\rangle$ is constructed by a sequence of $CZ_{i,j}$ gates acting on the state $|+\rangle^{\otimes n}$. Since CZ gates acting on different qubit pairs commute, the effect of all $CZ_{i,j}$ used to prepare $|G\rangle$ can be piecewise analyzed by examining the subset of CZ gates acting between different subsystems. For example, the edges in \mathcal{G} between vertex sets C and I are realized in $|\mathcal{G}\rangle$ by a set of circuits, one for each qubit in I . For each vertex $i \in I$, the edges connecting i to the center C are described by the i -th column of the block matrix CI , and correspond to a circuit U_i composed of $CZ_{c,i}$ gates, with $c \in C$. This correspondence between adjacency matrix columns and CZ gates establishes a dictionary between the vector algebraic and quantum circuit formalisms, complete with the following relations.

1. **Vector Addition:** Bitwise addition of two column vectors, i.e. $\mathbf{v}_i \oplus \mathbf{v}_j$, corresponds to applying their respective circuits sequentially $U_i U_j$.

2. **Column Space:** The column space $\text{Col}(CI)$, the linear span of CI columns, represents the set of all circuits built by multiplying smaller circuits $\{U_i\}_{i \in I}$. This set of “reachable circuits” forms a finite Abelian group.

The vector-circuit correspondence allows column space properties, such as intersection and distributivity, to be interpreted as physical properties of the entangling circuits that prepare the physical state. Moreover, this association highlights that non-local Clifford operations corresponding to elementary column operations, such as replacing a column \mathbf{v}_k with $\mathbf{v}_i \oplus \mathbf{v}_j$, preserve the column space of the associate adjacency block. In particular, any transformation that leaves the column spaces of CI , CJ , and CK invariant preserves the classification of $|\mathcal{G}\rangle$ for MMI_{CIJ} (4.8) given in Table 6, even though such transformations generally alter the state’s entropy vector (see Appendix A.3 for details).

4.3.2 The Physical Meaning of a Nontrivial Intersection

The necessary condition for the column spaces of CI , CJ , and CK to share a non-trivial intersection in order to fail MMI_{CIJ} (4.8), detailed in Observation 2, has direct physical implications in a quantum circuit framework. For block adjacency matrices CI , CJ , and CK , the condition $\text{Col}(CI) \cap \text{Col}(CJ) \cap \text{Col}(CK) \neq \emptyset$ implies that a vector exists which can be constructed independently from the columns of CI , from those of CJ , and from those of CK . In a quantum circuit framework, this criterion asserts that there must exist at least one entangling circuit, which we denote U_c , that can be constructed in three independent ways:

1. By multiplying the set of circuits $\{U_i\}_{i \in \alpha}$ where $\alpha \subseteq I$,
2. By multiplying the set of circuits $\{U_j\}_{j \in \beta}$ where $\beta \subseteq J$,
3. By multiplying the set of circuits $\{U_k\}_{k \in \gamma}$ where $\gamma \subseteq K$.

The graph state $|K_4\rangle$, represented by the four-star, illustrates the simplest possible construction of U_c . The MMI instances $|K_4\rangle$ fails are all of type MMI_{CIJ} (see Table 1), which is the special case of MMI_{CIJ} with $|C| = 1$. Thus, since $|K_4\rangle$ fails an MMI_{CIJ} , then, the preceding analysis ensures the existence of U_c for any valid tripartite subsystem $\{C = \{1\}, I, J\}$ of $|K_4\rangle$. We can see this trivially from the adjacency matrix of K_4 (3.13). The adjacency blocks relevant to MMI_{CIJ} that correspond to every tripartite subsystem $\{C = \{1\}, I, J\}$ of $|K_4\rangle$ are

$$CI = CJ = CK = [1], \quad (4.16)$$

which is the exact preparation of $|K_4\rangle$: a CZ between the central vertex $\{1\}$ and its leaves $\{2\}$, $\{3\}$, and $\{4\}$. In this case, we obtain the only nontrivial CZ circuit between two vertices.

Indeed, for states represented by graphs of type G , the existence of U_c is equivalent to the subgraph anchoring condition from Section 4.1. For graph states whose representation is of the \mathcal{G} family, the existence of U_c acts as a similar, though weaker, constraint to the subgraph anchoring. Using U_c , we can construct a state $|\mathcal{G}'\rangle$, using only transformations on $|\mathcal{G}\rangle$ that preserve the column spaces of CI, CJ and CK , where at least one qubit from each subsystem $i \in I, j \in J, k \in K$ shares identical connectivity with C . Importantly, while the state $|\mathcal{G}'\rangle$ may have a different entropy vector from $|\mathcal{G}\rangle$, its MMI_{CIJ} (4.8) evaluation is the same.

The construction of U_c above offers an interesting physical perspective. Given that subsystems I, J , and K are not directly connected by edges in \mathcal{G} , Observation 2 implies that MMI_{CIJ} (4.8) violation requires the existence of a vertex set $\{i, j, k, c\}$, with $i \in I, j \in J, k \in K$, and $c \in C$, such that

$$\mathcal{G}[\{i, j, k, c\}] \cong K_4. \quad (4.17)$$

Otherwise stated, the subgraph of \mathcal{G} induced by the vertices $\{i, j, k, c\}$ forms a four-star configuration.

For graphs of type \mathcal{G} , the presence of a K_4 subgraph is required for MMI_{CIJ} (4.8) violation. Consequently, arbitrary MMI_{CIJ} violations in $|\mathcal{G}\rangle$ must include (possibly recursive) compositions of this minimal MMI-violating subgraph (see Appendix A.3 for details). This principle holds if the core entanglement structure is preserved, i.e. the leaf vertices in each K_4 subgraph remain mutually disconnected within the graph. We highlight that the existence of a K_4 subgraph guarantees that there exists a partition under which the graph is (nontrivially) of type \mathcal{G} , since we can place the central vertex of K_4 in C , place each leaf of K_4 in I, J , and K , respectively, and place all remaining vertices of the graph in C .

4.3.3 The Physical Meaning of Distributivity

Column space distributivity constrains how information is shared from the center vertex set C to other subsystems. Consider a basis of $|C|$ independent and entangling operations $\mathcal{B} = \{B_1, B_2, \dots, B_C\}$. The basis \mathcal{B} generates all entanglement arrangements accessible by concatenations of $B \in \mathcal{B}$, comprised of CZ gates between the center C and any target qubit. The column spaces $\text{Col}(CI), \text{Col}(CJ)$, and $\text{Col}(CK)$ are then distributive if and only if every circuit reachable from the operations that built CI, CJ , and CK can be generated by a subset \mathcal{B} (details in Appendix A.2). For example, all circuits constructable from the operators that prepared adjacencies in CI may be generated by $\{B_1, B_3\}$, while the corresponding circuits constructable from the operators that prepared CJ are generated by $\{B_2, B_3, B_5\}$, and so forth.

The crucial feature underlying distributivity is that all three sets of circuits, constructable from CI, CJ , and CK , are built from subsets of the *same* basis. In a physical sense, this condition implies that the entanglement of I, J , and K with the

center C is not arbitrary, but is instead compactly generated from the same shared set of operations. This implication is bidirectional, allowing the generating subsets⁶ of \mathcal{B} to be deduced given the set of entangling circuits for CI , CJ , and CK .

4.4 MMI Failure for $|\mathcal{G}\rangle$ states is Not Fully Reducible to MMI_{CIJ} Failure

Our analysis thus far has focused on MMI_{CIJ} (4.8). However, we have observed, and explicitly verified up through $n = 8$ qubits, that the presence of a non-trivial intersection among column spaces CI , CJ , and CK in $|\mathcal{G}\rangle$, while not sufficient to ensure violation of MMI_{CIJ} (4.8) itself, is nevertheless sufficient to produce an MMI violation in some other subsystem of the same state. To illustrate this observation, consider the graph⁷ shown in Figure 9 which represents a state of type $|\mathcal{G}\rangle$ with non-distributive, intersecting column spaces for CI , CJ , and CK . This state $|\mathcal{G}\rangle$ satisfies MMI_{CIJ} (4.8) on the vertex sets C , I , and J shown in Figure 9. The specific subspace constructions are given in Table 10 (a) of Appendix A.2 under case ‘‘Satisfies’’, and a graph isomorphic to \mathcal{G} , which illustrates that Figure 9 is indeed a generalized star graph, is given in Table 8.

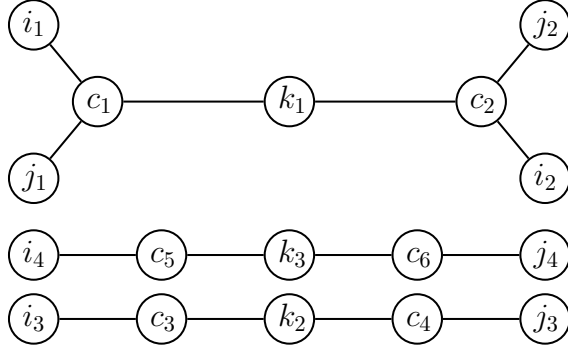


Figure 9. Graph representation for a state $|\mathcal{G}\rangle$ with nontrivial intersection among non-distributive subspaces $\text{Col}(CI)$, $\text{Col}(CJ)$, and $\text{Col}(CK)$, that satisfies MMI_{CIJ} (4.8). Vertex labels give subsystem membership $c_q \in C$, $i_q \in I$, $j_q \in J$, and $k_q \in K$.

While the full graph in Figure 9 satisfies MMI_{CIJ} (4.8), the uppermost subgraph containing vertices $\{c_1, c_2, i_1, i_2, j_1, j_2, k_1\}$ would fail MMI_{CIJ} (4.8) on its own by virtue of Observation 3. In fact, for every graph \mathcal{G} possessing a non-trivial intersection we find *some* violation of MMI on a subgraph of \mathcal{G} . While we have not successfully produced a generic proof of this conjecture, we have performed an exhaustive search

⁶In general, the full basis remains undetermined unless the union of the column spaces of CI , CJ , or CK is $\mathbb{Z}_2^{|C|}$. Nevertheless, we can always deduce the generating subsets in a compatible basis.

⁷While this graph is disconnected, the missing edges do not impact MMI_{CIJ} (4.8) (see Eq. (4.10)). Furthermore, connecting vertices k_1 , k_2 , and k_3 does not alter the satisfaction of MMI_{CIJ} (4.8). The graph remains MMI-violating, since it becomes a graph of the form G .

up through 8 qubits.⁸ When a nontrivial intersection was identified, we provide the specific choice of C , I , and J that contains the largest number of elements still satisfying this condition. All states obtained through this procedure are of type $|\mathcal{G}\rangle$ under the indicated partition. Among the 46 MMI-satisfying graphs in Table 11, none exhibit a nontrivial intersection, nor do any states in their respective LC orbits. Of the 136 MMI-failing graphs for each entropy vector, Table 13 reveals that 8 fail MMI despite not having a nontrivial intersection for any valid choice of C , I , and J . Table 9 presents example graphs from Tables 11–13; clicking on the label of each graph redirects to an applet that provides access to the entropy vector of its corresponding state.

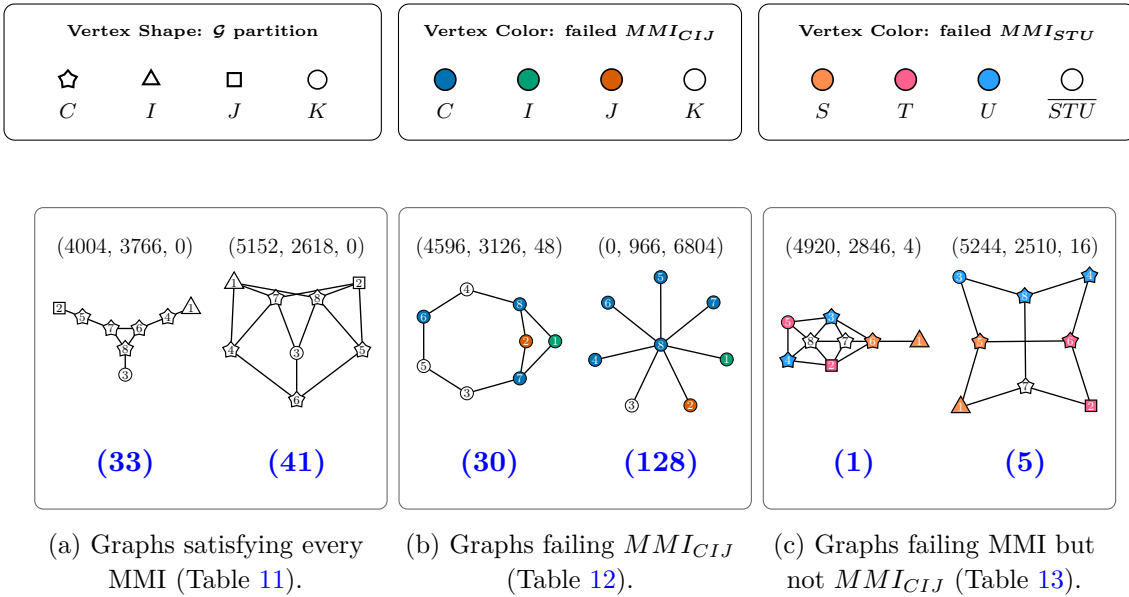


Table 9. Graph examples from the classification of star graphs \mathcal{G} realizing all unique eight-qubit entropy vectors, organized by MMI failure and the presence of a nontrivial intersection (see Tables 11–13 for the full classification). Vertex shape encodes a partition defining each \mathcal{G} , and vertex color marks a failing MMI instance; in Table 9 these two partitions coincide, so we indicate it only by coloring. MMI evaluation counts are given as the ordered triple (Satisfies, Saturates, Fails), with each entry equal to the number of instances yielding that outcome. Clicking each graph’s label redirects to a website that provides easy access to the entropy vector of its state.

We present the following observations from the data⁹, which found no counterexamples in an exhaustive search through eight qubits; limited exploration at nine and

⁸The graph labeled (1) in Table 13 is the only exception, as we chose an LC orbit representative with an induced four-star rather than the minimal-edge one.

⁹All data is available and reproducible from *Mathematica* notebooks in [35]. We give code for graph and tableau representations of stabilizer states, functions to generate/transform states, compute entropy vectors and symmetries, and evaluate entropy inequalities. The repository includes data for Appendix B on MMI failure for stabilizer states through seven qubits,

ten qubits has also yielded no counterexamples. Tables 11-13 list MMI-satisfying and MMI-failing graphs, respectively, for each of the 182 entropy vectors of stabilizer states at $n = 8$, unique up to symmetry [36]. For each representative graph G , we generated and searched its full LC orbit to identify a minimal-edge given in Tables 11-13.

Observation 5. *Every graph state, up to $n = 8$, is LC -equivalent to a $|\mathcal{G}\rangle$ state for some partition.*

Observation 6. *The property that $|\mathcal{G}\rangle$ has a nontrivial intersection among the column spaces CI , CJ , and CK , for some valid choice of $\{C, I, J\}$, is not LC -invariant.*

Observation 7. *Although every MMI-violating graph, up to $n = 6$, is LC -equivalent to a \mathcal{G} graph with nontrivial intersection on the column spaces CI , CJ , and CK , this condition is not necessary for generic MMI failure on $|\mathcal{G}\rangle$.*

Observation 8. *Possessing a nontrivial intersection of the column spaces CI , CJ , and CK is a sufficient condition for the failure of **some** MMI instance, though not that specific MMI_{CIJ} , in $|\mathcal{G}\rangle$ states. Table 11 confirms this observation for $|\mathcal{G}\rangle$ up through $n = 8$.*

Observation 9. *Path and cycle graphs, which never realize a nontrivial intersection, as well as specific combinations of path and cycle graphs, form families of graphs that never fail MMI. Table 11 confirms this observation for $|\mathcal{G}\rangle$ up through $n = 8$.*

We now conclude the series of observations from Tables 11-13 with a forbidden-subgraph conjecture. In Section 4.3.2, we showed that the necessary condition 2 for MMI_{CIJ} violation in a graph state $|\mathcal{G}\rangle$ implies that \mathcal{G} contains an induced four-star. Therefore, we expect, and indeed observe, every graph in Table 12 to have an induced four-star. Additionally, we can explicitly observe the graphs in Table 13, which are of type \mathcal{G} and fail MMI not of type MMI_{CIJ} (4.8), to have an induced four-star as well. Moreover, we confirmed Observation 9 exhaustively up to $n = 10$, providing further evidence that path and cycle graphs—whose maximal vertex connectivity is 2 and which therefore contain no induced four-star—appear to be graph families that never fail MMI (2.5).

Ultimately, these computational and analytic observations provide evidence that an induced four-star may be necessary for violating *any* MMI (2.5) inequality, motivating the conjecture that any MMI-violating graph state has some graph representation containing a K_4 graph. Then, by the argument in the paragraph following Eq. (4.17), there is a partition under which that graph representation is nontrivially type \mathcal{G} . Formally, we conjecture the following:

Conjecture 1 (Forbidden-Subgraph). *Any graph state that violates MMI (2.5) has a graph representation that is LC -equivalent to a graph H containing a K_4 subgraph. H is \mathcal{G} with respect to some partition.*

In this section, we developed a framework for identifying and characterizing specific MMI violations in graph states. We proved that graphs of type G , a single central vertex c connected to mutually disjoint and disconnected subgraphs, necessarily violate MMI_{cIJ} (4.2). We then generalized this construction to consider graphs of type \mathcal{G} , where the vertex c is promoted to a multi-vertex subgraph C . In this generalization, we derived conditions to determine whether states $|\mathcal{G}\rangle$ satisfy, saturate, or fail MMI_{CIJ} , based on the intersection and distributive properties adjacency submatrix column spaces in \mathcal{G} . Summarized in Table 6, our classification revealed that a nontrivial intersection among these column spaces is necessary, and when combined with distributivity is sufficient to produce MMI_{CIJ} violation.

Physically, the algebraic relations derived in this section correspond to the existence of shared entangling circuits between subsystems, with MMI_{CIJ} failure linked to the presence of a K_4 subgraph. We conjectured that every MMI-violating stabilizer state is LC -equivalent to a generalized star graph \mathcal{G} under *some* partition. We exhaustively verify this conjecture up through $n = 8$ qubits, though the conjecture may hold at higher qubit number. We now conclude by discussing broader implications and extensions of these results.

5 Discussion: Toward a Complete Characterization of MMI Violation in Stabilizer States

In this work, we progress towards a complete characterization of monogamy of mutual information (MMI) violation for graph states by identifying algebraic conditions on adjacency matrices that determine the evaluation of specific MMI instances. We first present a family of graphs G , composed of disjoint subgraphs connected only through a single-vertex center c (shown in Figure 7), and prove that the associated graph states $|G\rangle$ will always fail the set of MMI instances MMI_{cIJ} , defined in Eq. (4.2). The set of MMI instances MMI_{cIJ} is defined by a pairwise disjoint tripartite subsystem $(\{c\}, I, J)$, with a nonempty complement K , such that all paths between I and J must include only c .

We next extend our analysis to the broader class of generalized star graphs \mathcal{G} , in which the central node c is promoted from a single vertex to an arbitrary subgraph C . Unlike $|G\rangle$, the corresponding graph states $|\mathcal{G}\rangle$ are not guaranteed to violate MMI_{CIJ} based solely on their star-like graph topology. We therefore provide a complete characterization of MMI_{CIJ} evaluation for any $|\mathcal{G}\rangle$, expressed in terms of the algebraic structure of adjacency submatrices that encode nontrivial adjacencies between elements in the partition $\{C, I, J, K\}$. The essential features are captured by matrix subblocks CI , CJ , and CK , which we systematically classify in Table 6 and summarize by the following.

1. A nontrivial intersection of the column spaces of CI , CJ , and CK is a *necessary* condition to violate MMI_{CIJ} .
2. Requiring that intersections distribute over subspace sums, for the column spaces of CI , CJ , and CK , gives a *sufficient* condition for MMI_{CIJ} violation.
3. Configurations which are both trivially intersecting and distributive guarantee saturation of MMI_{CIJ} , whereas trivially intersecting and non-distributive configurations strictly satisfy MMI_{CIJ} .
4. Configurations with a non-trivial intersection and non-distributive column spaces are unconstrained in their MMI_{CIJ} evaluation.

For each case in the above categorization, we provide an explicit graph construction in Tables 7 and 8.

Our analysis focused on MMI violations in graph states, providing a complete characterization of MMI_{CIJ} evaluation for generalized star graphs \mathcal{G} . Nevertheless, computational evidence identifies graph states that fail MMI while possessing no single nontrivial intersection, nor any such intersection in their full LC orbit, for any valid choice of $\{C, I, J\}$ (see Table 13). These examples therefore demonstrate MMI violations not captured by the presence of a star graph structure.

The analysis techniques developed in this work can, in principle, be extended to explore generic MMI instances, enabling a fully general study of MMI failure in graph states. The primary challenge for this extension is that, for general MMI instances, the relevant submatrix ranks involve decomposing the rank of a 2×2 block matrix, preventing a simplification analogous to Eq. (A.4). Further work might seek to alternatively express the ranks of block matrices in terms of their blocks, thereby avoiding recursive applications of the subspace addition formula in Eq. (A.2). Additional approaches include leveraging rank-exposing decompositions, or related matrix identities that enable the simplification of block matrix rank into an amenable form, ultimately facilitating a general framework for studying MMI violation.

This work establishes a correspondence between the algebraic features that determine MMI evaluation for graph states, and the operators used to prepare such states. A nontrivial intersection among the column spaces of CI , CJ , and CK implies the existence of an operator that can be constructed independently of the operators used to entangle each pair of subsystems. Distributivity, meanwhile, reveals a higher degree of organization: there exists a minimal generating set of operators for all entanglement patterns between qubits and the center C , whose subsets reproduce the entangling operators for CI , CJ , and CK individually.

One natural follow-up to this work is to characterize MMI failure for the graph states shown in Table 13, which satisfy all MMI_{CIJ} instances under which they are \mathcal{G} graphs. However, these states still violate MMI instances, just not ones under which

there is an LC orbit member that is \mathcal{G} . For example, graph (1) in Table 13 fails instances $MMI_{\{16, 25, 34\}}$, $MMI_{\{16, 34, 78\}}$, and $MMI_{\{25, 34, 78\}}$, with $MMI_{\{16, 25, 34\}}$ colored in the figure. Up to symmetry, the unique instances failed are $MMI_{\{16, 25, 34\}}$ and $MMI_{\{25, 34, 78\}}$, out of the 7770 distinct MMI instances that exist at $n = 8$ qubits. Comparing these MMI failures, e.g. $MMI_{\{16, 25, 34\}}$ and $MMI_{\{25, 34, 78\}}$, to those observed in the graphs of Table 12, which violate the chosen MMI_{CIJ} , may provide insights towards a complete characterization of MMI violation in graph states.

The correspondence between entropy inequality evaluation and the algebraic structure of adjacency matrix components extends beyond MMI. Higher-party holographic inequalities are especially appealing targets given their physical relevance and inherent symmetry. All holographic entropy inequalities are balanced, meaning each subsystem appears the same number of times on each side of the inequality [19, 37, 38]. The methods introduced in this work are particularly effective for evaluating such inequalities on generalized star graphs, as the subgraph disjointness condition (3) ensures that each entropy reduces to the rank of a single row of block matrices for inequalities analogous to MMI_{CIJ} . Rewriting these inequalities using the adjacency matrix rank expression in Eq. (2.19), and applying the subspace dimension addition relation, allows the inequality to be completely expressed in terms of intersection dimensions of specific subspaces. For balanced inequalities on N regions, such as those constraining the entropy vectors for holographic states, all individual submatrix ranks cancel. This reformulation should enable the systematic exploration of a broader set of entropy inequalities using the same techniques presented herein.

The discovery of the graphs G , shown in Figure 7, was inspired by the repeated appearance of a four-star subgraph within the LC orbit of graph states that fail MMI. We formalized why generalized star graphs fail MMI, by establishing the necessary condition of a nontrivial intersection in Observation 2. Interestingly, even certain graph states that do not violate MMI_{CIJ} contain the same “forbidden” four-star in their LC orbits (see Table 13). This observation motivates the forbidden-subgraph conjecture, stated in Conjecture 1, which posits the *necessity* of an induced four-star in the LC orbit of any graph whose associated graph state violates MMI . This conjecture realizes every MMI-violating stabilizer entropy vector as a graph state $|\mathcal{G}\rangle$, since containment of a K_4 subgraph is sufficient for a graph to be of type \mathcal{G} (see Section 4.3.2).

If an induced four-star in the LC orbit is indeed necessary for any MMI failure, it becomes compelling to ask whether the empirical observation that MMI violations precede other holographic entropy inequality violations for $n \leq 6$ [39] is coincidental or structural. If higher-party violations decompose into their minimal violators, refined versions of our methods, which would account for MMI failure in general, could be used to test whether MMI failure is necessary for *all* higher-party violations.

For $n \leq 8$ qubits, as shown in Figures 11 and 12, a nontrivial intersection of the

column spaces of CI , CJ , and CK (Observation 2) appears not only necessary for failure of MMI_{CIJ} but also sufficient to guarantee failure of *some* MMI instance. The challenge in proving the sufficiency of a nontrivial intersection for MMI failure lies in managing the edge cases across all MMI instances whose outcome can be determined only by this algebraic requirement.

The methods established in this work apply directly to graph states and, by local Clifford equivalence, to stabilizer states [27]. The algebraic conditions derived herein could be extended from qubits to qudit systems, potentially offering insights into state preparation where unitary operators that prepare states and entropies are expressed using a directed graph representation [40, 41]. Our calculations in this work rely on an adjacency-matrix computation for entanglement entropy, as in Eq. (2.19). If such a formula holds for directed graph representations, then our methods apply equivalently. Moreover, this framework provides a bridge to studying non-stabilizer resources based in entropy calculations [42], i.e. such as stabilizer Renyi entropy [43] or non-local quantum magic [44, 45], relating their structure to entanglement-based diagnostics, e.g. capacity of entanglement [46–48] or operator entanglement [49], to capture deviations from stabilizerness.

Figures 11–13 demonstrate that every graph state, for $n \leq 8$, is LC-equivalent to a graph that is a generalized star under some partition as indicated for each graph. Nevertheless, the property of being \mathcal{G} under a given partition is not invariant under LC transformations. Moreover, at $n = 9$ qubits and above, two graph states which are not LC-equivalent can share the same entropy vector [50, 51]. Accordingly, it remains an open question whether *every* graph is LC-equivalent to a nontrivial generalized star. As we note in Section 4.2, this question reduces to proving that every graph state on $n \geq 4$ vertices is LC-equivalent to a graph with some 4-vertex subset inducing an empty graph. If true, then generalized star graphs would enable an efficient canonical form for exploring the stabilizer entropy vector space.

The property of having a nontrivial intersection of the column spaces of CI , CJ , and CK , as in Observation 2, is not an LC invariant statement, as we demonstrate in the construction of Figures 11–13. A natural extension of this work is to formulate an LC-invariant version of the necessary condition for MMI_{CIJ} failure, and ultimately to characterize the failure of all MMI instances.

A deeper understanding of MMI violation in graph states provides a tool for advancing both the theoretical foundations and practical implementation of future quantum networks. Many contemporary approaches to near-term quantum networks adopt a graph state model [52–55], where network nodes correspond to graph vertices and entanglement is shared through physical channels, e.g. optical fibers. Once initialized, these long-range entangled states enable a wide range distributed computing tasks, from entanglement sharing [4, 23, 24, 56, 57] to quantum key distribution [58–61]. Characterizing how MMI evaluation is impacted by the underlying entanglement structure of the graph, and equivalently the associated network topol-

ogy, informs how entanglement can be shared, localized, and redistributed among different network nodes. These insights inform the development of more robust and resource-efficient network protocols, providing direct technological applications for the constraints imposed by entropy inequalities.

Acknowledgments

The authors thank Adam Burchardt, Bartek Czech, William Kretschmer, and Monica Kang for helpful conversations. C. K. is supported by the U.S. Department of Energy under grant number DESC0019470 and by the Heising-Simons Foundation “Observational Signatures of Quantum Gravity” collaboration grants 2021-2818 and 2024-5305, and W.M. and J.F. have also been supported by 2021-2818. W.M. is supported by the Department of Energy (DOE) Office of Science (SC) Grant No DOE DE-FOA-0003432 and by Grant No GBMF12976 of the Gordon and Betty Moore Foundation. This work was performed in part at the Aspen Center for Physics, which is supported by National Science Foundation grant PHY-2210452.

A Additional Derivations and Proofs

A.1 Expressing MMI_{CIJ} as the Dimension of Column Spaces of Adjacency Submatrices

Recall that for any matrix M ,

$$\text{rank}(M) = \dim \{\text{Col}(M)\}, \quad (\text{A.1})$$

where $\text{Col}(M)$ denotes the column space of M , which is the subspace spanned by the columns of M . Moreover, for any linear subspaces W_1 and W_2 ,

$$\dim \{W_1 + W_2\} = \dim \{W_1\} + \dim \{W_2\} - \dim \{W_1 \cap W_2\}. \quad (\text{A.2})$$

Thus, every entropy involved in MMI_{CIJ} (4.8) can be expressed as follows:

$$\begin{aligned} S_C &= \text{rank} \left(\begin{bmatrix} CI & CJ & CK \end{bmatrix} \right) \\ &= \text{rank} \left(\begin{bmatrix} CI & CJ \end{bmatrix} \right) + \text{rank}(CK) \\ &\quad - \dim \{(\text{Col}(CI) + \text{Col}(CJ)) \cap \text{Col}(CK)\} \\ &= \text{rank}(CI) + \text{rank}(CJ) + \text{rank}(CK) \\ &\quad - \dim \{\text{Col}(CI) \cap \text{Col}(CJ)\} - \dim \{(\text{Col}(CI) + \text{Col}(CJ)) \cap \text{Col}(CK)\}, \\ S_I &= \text{rank}(CI), \\ S_J &= \text{rank}(CJ), \\ S_{CIJ} &= \text{rank}(CK), \\ S_{CI} &= \text{rank}(CJ) + \text{rank}(CK) - \dim \{\text{Col}(CJ) \cap \text{Col}(CK)\}, \\ S_{CJ} &= \text{rank}(CI) + \text{rank}(CK) - \dim \{\text{Col}(CI) \cap \text{Col}(CK)\}, \\ S_{IJ} &= \text{rank}(CI) + \text{rank}(CJ) - \dim \{\text{Col}(CI) \cap \text{Col}(CJ)\} \end{aligned} \quad (\text{A.3})$$

The entropies above allow us to express MMI_{CIJ} as:

$$\begin{aligned} &\dim \{\text{Col}(CI) \cap \text{Col}(CK)\} + \dim \{\text{Col}(CJ) \cap \text{Col}(CK)\} \\ &\leq \dim \{(\text{Col}(CI) + \text{Col}(CJ)) \cap \text{Col}(CK)\}. \end{aligned} \quad (\text{A.4})$$

A.2 A Classification of $|\mathcal{G}\rangle$ According to MMI Evaluation Based on the Properties of the Block Elements of $\Gamma^{\mathcal{L}}$

Let W_1, W_2 , and W_3 denote arbitrary subspaces of a vector space V . From the dimension formula for the sum of two subspaces (A.2), it follows:

$$\dim \{W_1 \cap W_3 + W_2 \cap W_3\} = \dim \{W_1 \cap W_3\} + \dim \{W_2 \cap W_3\} - \dim \{W_1 \cap W_2 \cap W_3\}. \quad (\text{A.5})$$

Additionally, the subspace inclusion

$$W_1 \cap W_3 + W_2 \cap W_3 \subseteq (W_1 + W_2) \cap W_3, \quad (\text{A.6})$$

implies the following general inequality:

$$\dim \{W_1 \cap W_3\} + \dim \{W_2 \cap W_3\} - \dim \{W_1 \cap W_2 \cap W_3\} \leq \dim \{(W_1 + W_2) \cap W_3\}. \quad (\text{A.7})$$

Equality in (A.7) holds precisely under the condition

$$W_1 \cap W_3 + W_2 \cap W_3 = (W_1 + W_2) \cap W_3, \quad (\text{A.8})$$

which is known as distributivity. If distributivity holds, it remains valid under any permutation of the subspaces. As established in [62, Section 1.7], a collection of subspaces W_1, \dots, W_N of V is distributive if and only if there exists a common basis \mathcal{B} of V such that

$$W_i = \langle B_i \rangle, \quad B_i \subseteq \mathcal{B}, \quad \text{for } i \in \{1, \dots, N\}, \quad (\text{A.9})$$

where $\langle B_i \rangle$ denotes the linear span of B_i .

We now examine exhaustively all evaluations of the inequality (A.7) according to the algebraic structures of the subspaces W_1, W_2 , and W_3 .

Case 1. W_1, W_2, W_3 are *non-distributive* with $\dim \{W_1 \cap W_2 \cap W_3\} = 0$: In this case, Eq. (4.11) simplifies to

$$\dim \{W_1 \cap W_3\} + \dim \{W_2 \cap W_3\} < \dim \{(W_1 + W_2) \cap W_3\}. \quad (\text{A.10})$$

Case 2. W_1, W_2, W_3 are *distributive* with $\dim \{W_1 \cap W_2 \cap W_3\} = 0$: Then, equality holds exactly as:

$$\dim \{W_1 \cap W_3\} + \dim \{W_2 \cap W_3\} = \dim \{(W_1 + W_2) \cap W_3\}. \quad (\text{A.11})$$

Case 3. W_1, W_2, W_3 are *distributive* with $\dim \{W_1 \cap W_2 \cap W_3\} > 0$: Here, dimensional subadditivity ensures the strict inequality

$$\dim \{W_1 \cap W_3\} + \dim \{W_2 \cap W_3\} > \dim \{W_1 \cap W_3 + W_2 \cap W_3\}. \quad (\text{A.12})$$

Since the subspaces are distributive $W_1 \cap W_3 + W_2 \cap W_3 = (W_1 + W_2) \cap W_3$, then

$$\dim \{W_1 \cap W_3\} + \dim \{W_2 \cap W_3\} > \dim \{(W_1 + W_2) \cap W_3\}. \quad (\text{A.13})$$

Case 4. W_1, W_2, W_3 are *non-distributive* with $\dim \{W_1 \cap W_2 \cap W_3\} > 0$: Under these assumptions, we examine the inequality

$$\dim \{W_1 \cap W_3\} + \dim \{W_2 \cap W_3\} \leq \dim \{(W_1 + W_2) \cap W_3\}. \quad (\text{A.14})$$

All previously considered conditions, namely, strict satisfaction (A.10), saturation (A.11), and failure (A.13), remain possible for inequality (A.14). To provide explicit constructions that realize each possibility, we set $V = \mathbb{Z}_2^6$ as the ambient vector space containing subspaces W_1 , W_2 , and W_3 . Let $\mathcal{B} = \{e_1, e_2, e_3, e_4, e_5, e_6\}$ be a fixed basis of \mathbb{Z}_2^6 . Table 10 provides an example of a Case 4 construction for W_1 , W_2 , and W_3 that illustrates these distinct possibilities concerning inequality (A.14).

(a) Subspace Construction			
Evaluation	W_1	W_2	W_3
ST	$\langle e_1, e_2 \rangle$	$\langle e_1, e_3 \rangle$	$\langle e_1, e_2 + e_3 \rangle$
F	$\langle e_1, e_3, e_4 \rangle$	$\langle e_2, e_3, e_4 \rangle$	$\langle e_1 + e_2, e_3, e_4 \rangle$
S	$\langle e_1, e_2, e_3, e_5 \rangle$	$\langle e_1, e_2, e_4, e_6 \rangle$	$\langle e_1 + e_2, e_3 + e_4, e_5 + e_6 \rangle$

(b) Intersections			
Evaluation	$W_1 \cap W_3$	$W_2 \cap W_3$	$(W_1 + W_2) \cap W_3$
ST	$\langle e_1 \rangle$	$\langle e_1 \rangle$	$\langle e_1, e_2 + e_3 \rangle$
F	$\langle e_3, e_4 \rangle$	$\langle e_3, e_4 \rangle$	$\langle e_1 + e_2, e_3, e_4 \rangle$
S	$\langle e_1 + e_2 \rangle$	$\langle e_1 + e_2 \rangle$	$\langle e_1 + e_2, e_3 + e_4, e_5 + e_6 \rangle$

Table 10. Example constructions of subspaces $W_1, W_2, W_3 \subseteq \mathbb{Z}_2^6$ are provided, illustrating saturation (ST), failure (F), and satisfaction (S) with respect to inequality (A.14). The vectors $\{e_i\}_{i=1}^6$ form a fixed basis of the ambient space \mathbb{Z}_2^6 . The notation $\langle e_1, \dots, e_k \rangle$ denotes the linear span of $\{e_1, \dots, e_k\}$.

Specializing the preceding discussion by setting $W_1 = W_I$, $W_2 = W_J$, and $W_3 = W_K$ as subspaces of $V = \mathbb{Z}_2^{|C|}$, one directly obtains the MMI evaluation corresponding to each subclass of \mathcal{G} detailed in Table 6. Table 7 presents example graphs corresponding to the first three cases in Table 6, while Table 8 presents graphs that realize each Case 4 evaluation example in Table 10 (a).

A.3 Deducing the Claims in Section 4.3

Proposition 2. *Operations on $|\mathcal{G}\rangle$ that act invariantly on $\text{Col}(CI)$, $\text{Col}(CJ)$ and $\text{Col}(CK)$:*

1. *Leave every entropy of $|\mathcal{G}\rangle$ in MMI_{CIJ} invariant.*
2. *Preserve the MMI_{CIJ} evaluation and classification of $|\mathcal{G}\rangle$.*
3. *Generally alter the entropy vector of $|\mathcal{G}\rangle$.*

Proof. The first statement of the proposition follows immediately from the equation block (A.3). This block contains every entropy involved in MMI_{CIJ} (4.8), and shows

that they are expressed only in terms of $\text{Col}(CI)$, $\text{Col}(CJ)$, and $\text{Col}(CK)$. Consequently, operations that preserve $\text{Col}(CI)$, $\text{Col}(CJ)$, and $\text{Col}(CK)$ simultaneously leave every entropy involved in MMI_{CIJ} invariant.

The second statement follows immediately from the first, as if every entropy in MMI_{CIJ} is preserved, its evaluation will remain invariant. Furthermore, MMI_{CIJ} classification per Table 6 is exclusively made in terms of $\text{Col}(CI)$, $\text{Col}(CJ)$, and $\text{Col}(CK)$, meaning that their algebraic properties such as distributivity and intersections will be unchanged if these subspaces are also unchanged.

The third statement is a consequence of column operations on CI , CJ , and CK , which preserve their column spaces, being realized on $|\mathcal{G}\rangle$ as a sequence of CZ operations, which are non-local. In a given partition of $|\mathcal{G}\rangle$ specified by $\{C, I, J\}$, we can apply focalized transformations that correspond to column operations on $|\mathcal{G}\rangle$ that preserve, $\text{Col}(CI)$, $\text{Col}(CJ)$, and $\text{Col}(CK)$, separately, since I, J and K are pairwise disjoint subsystems. Nevertheless, these transformations could alter the column space of the complete adjacency matrix of \mathcal{G} , possibly changing the entropy vector of $|\mathcal{G}\rangle$. \square

Proposition 3. *Every unique failure of MMI_{CIJ} for states of type $|\mathcal{G}\rangle$ is realized by a graph state whose representation only admits star graphs.*

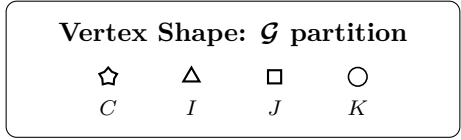
Proof. From Eq. (A.3), all entropies needed to evaluate MMI_{CIJ} (4.8) are independent of the self adjacency blocks CC, II, \dots of each element in the partition $\{C, I, J, K\}$. Thus, we may fix these regions having no internal adjacencies, and still be able to obtain any portion of any graph state entropy vector that produces any outcome for MMI_{CIJ} instances. Under such an assumption, the construction of \mathcal{G} (conditions (1) and (3)) ensures we obtain a graph composed exclusively of the disjoint union of n -stars, K_n , which completes the proof. \square

A.4 Graph Representatives for Every Stabilizer State Entropy Vector at $n = 8$ Qubits, up to Symmetry, and Their MMI Evaluations

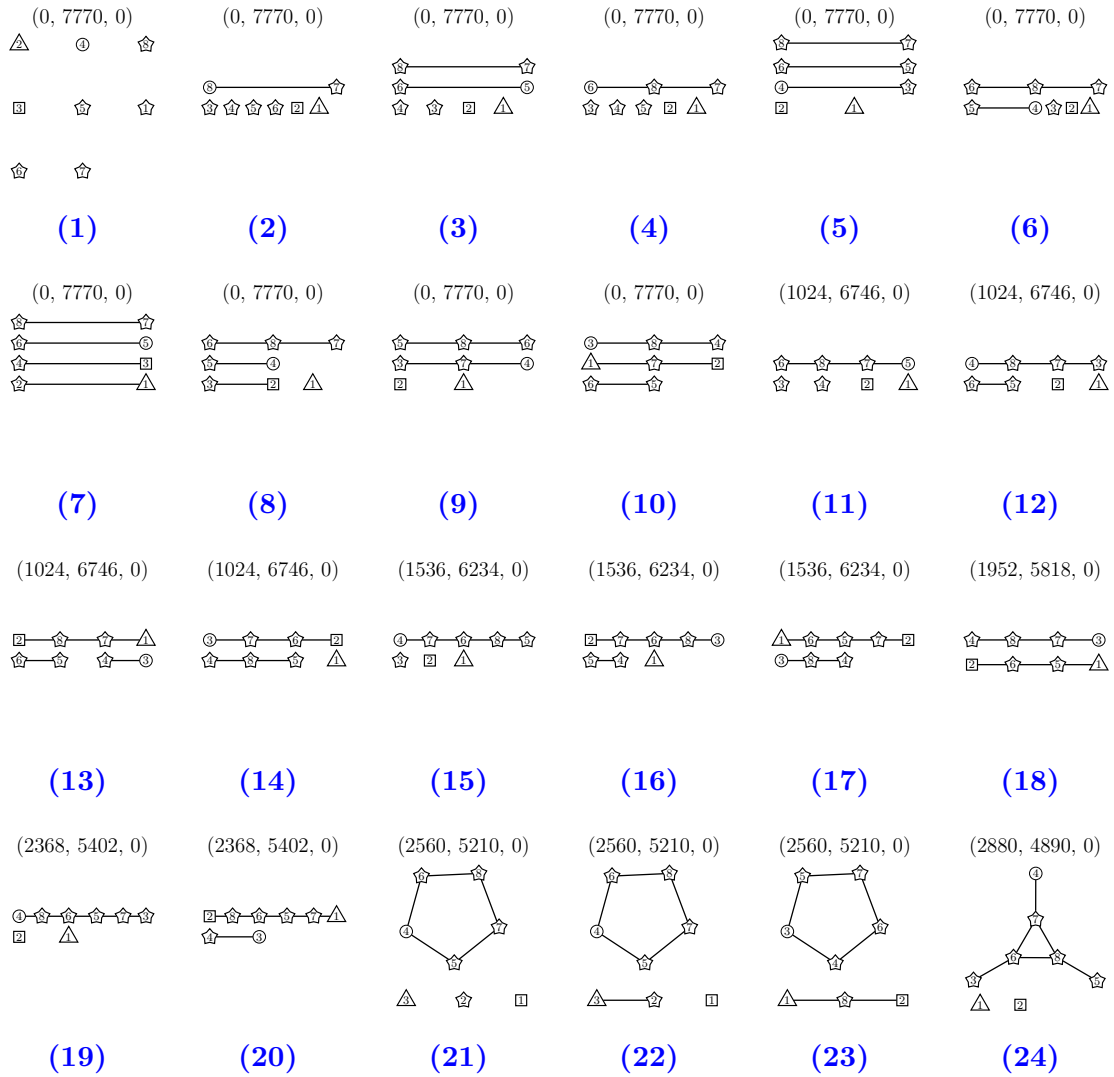
This section presents a graph representative for each of the 182 eight-qubit stabilizer-state entropy vectors [36], unique up to qubit exchange. We chose each representative to be \mathcal{G} under the specified partition $\{C, I, J, K\}$. We classify these graphs into three categories, according to the MMI behavior of their associated graph states:

1. Those that satisfy all MMI instances (Table 11);
2. Those that fail MMI_{CIJ} and are \mathcal{G} , necessarily with a nontrivial intersection for the partition $\{C, I, J, K\}$ (Table 12);
3. Those that fail MMI but do not exhibit a nontrivial intersection for any choice of $\{C, I, J\}$ under which the graph is \mathcal{G} (Table 13).

No eight-qubit graph state that satisfies MMI possesses a nontrivial intersection for any $\{C, I, J\}$ under which it is nontrivially \mathcal{G} . Each graph representative was selected as the minimal-edge representative of its local Clifford (LC) orbit within its category. The full dataset, along with a detailed tutorial explaining how to reproduce the results and use the accompanying *Mathematica* notebook, is available in the GitHub repository [35].



Clicking each graph's label redirects to a website that provides easy access to the entropy vector of its state.



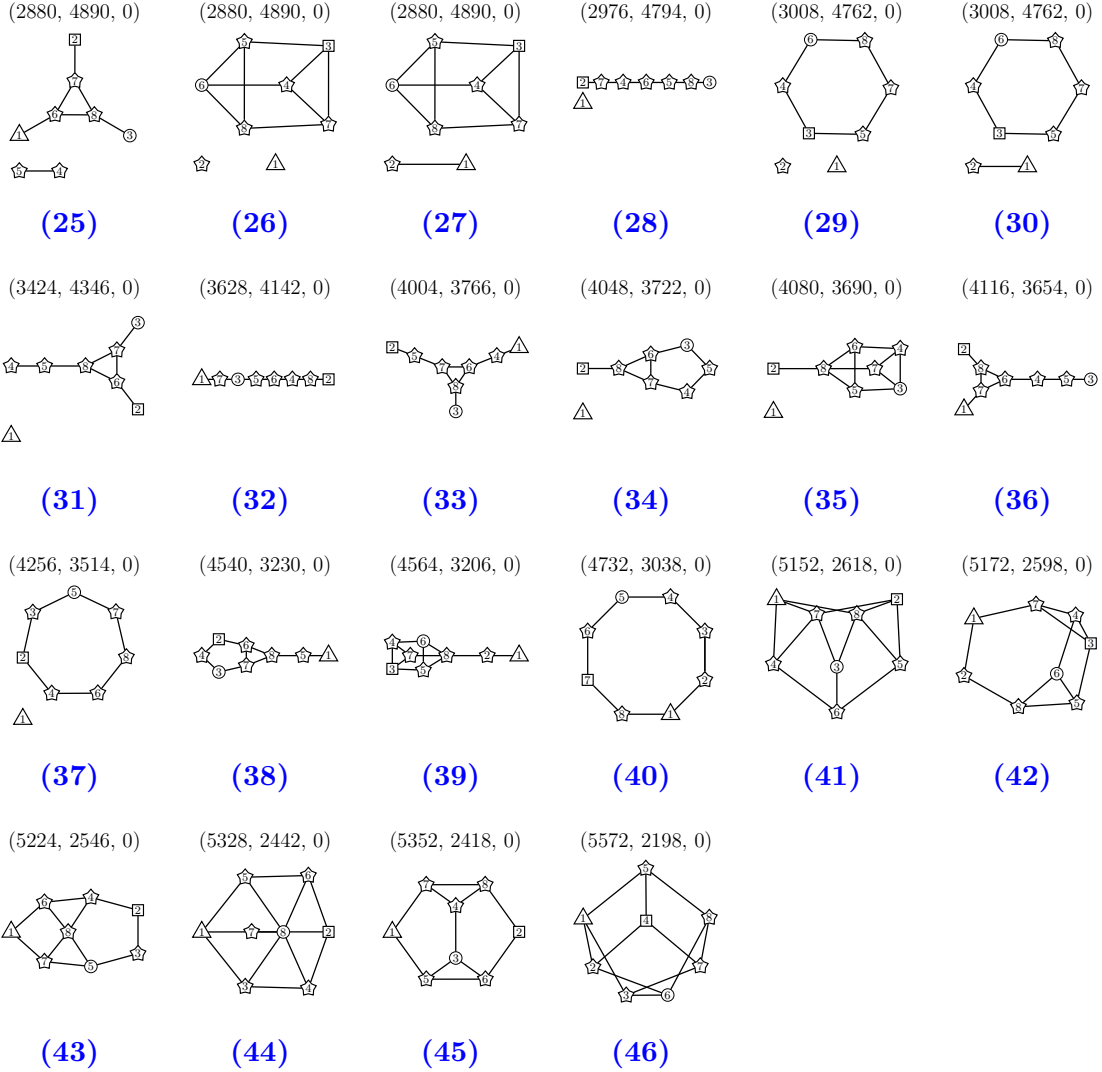
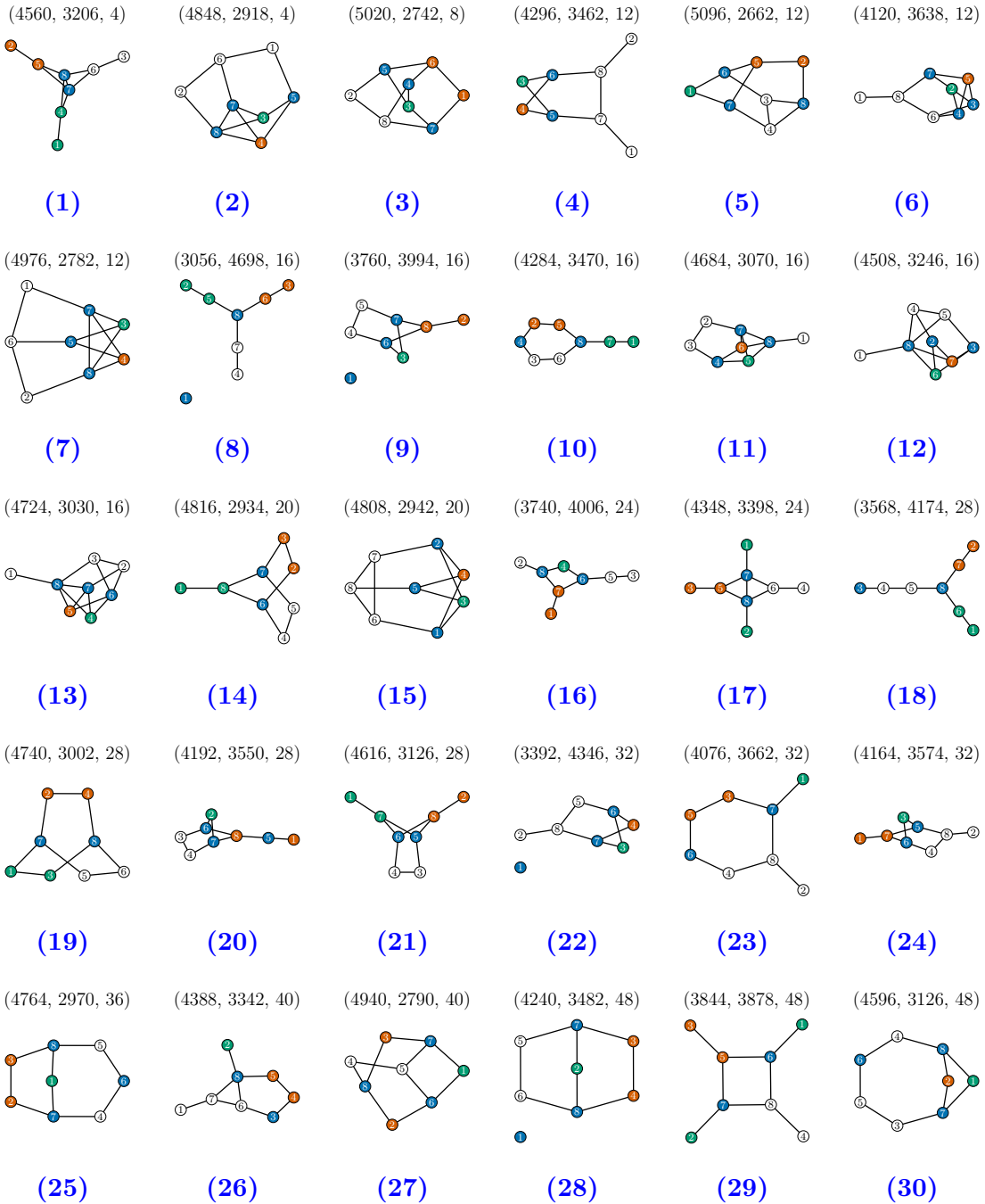


Table 11: Minimal-edge \mathcal{G} representatives of each entropy vector, unique up to symmetry at $n = 8$, corresponding to states that do not violate any MMI instance, with vertex shape encoding a partition $\{C, I, J, K\}$. An exhaustive search of the LC orbit of each representative found no choices of $\{C, I, J\}$ such that the column spaces of CI, CJ , and CK intersected non-trivially. MMI evaluation counts are listed in the form (Satisfies, Saturates, Fails), each entry giving the MMI instance count yielding the respective outcome. Graphs are enumerated in increasing order of satisfied MMI instances, with edge count and graph diameter serving as tie-breakers, in that order.

Vertex Color: failed MMI_{CIJ}

●	●	●	○
C	I	J	K

Clicking each graph's label redirects to a website that provides easy access to the entropy vector of its state.

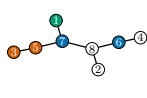


(3744, 3974, 52)



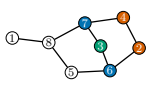
(31)

(3044, 4670, 56)



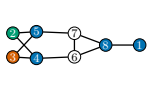
(32)

(4588, 3126, 56)



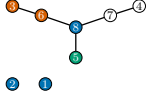
(33)

(4356, 3358, 56)



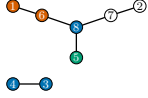
(34)

(2048, 5658, 64)



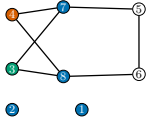
(35)

(2048, 5658, 64)



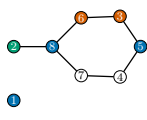
(36)

(2816, 4890, 64)



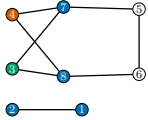
(37)

(3408, 4298, 64)



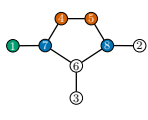
(38)

(2816, 4890, 64)



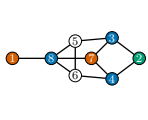
(39)

(4000, 3702, 68)



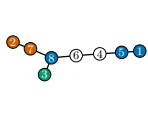
(40)

(4740, 2958, 72)



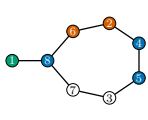
(41)

(3200, 4494, 76)



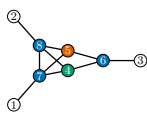
(42)

(4284, 3406, 80)



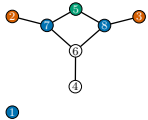
(43)

(3908, 3782, 80)



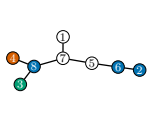
(44)

(2752, 4922, 96)



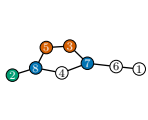
(45)

(2212, 5454, 104)



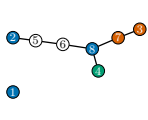
(46)

(3900, 3766, 104)



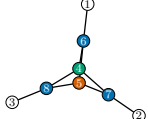
(47)

(2352, 5306, 112)



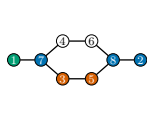
(48)

(3680, 3974, 116)



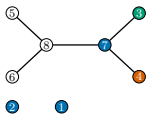
(49)

(3772, 3878, 120)



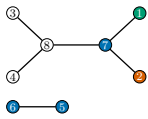
(50)

(576, 7066, 128)



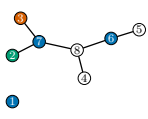
(51)

(576, 7066, 128)



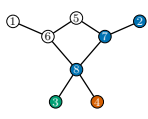
(52)

(1824, 5818, 128)



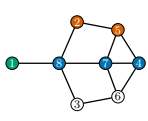
(53)

(2456, 5166, 148)



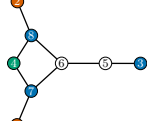
(54)

(4404, 3206, 160)



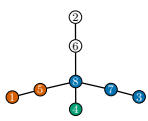
(55)

(3100, 4502, 168)



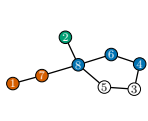
(56)

(2796, 4790, 184)



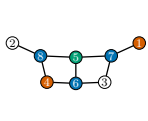
(57)

(3452, 4134, 184)



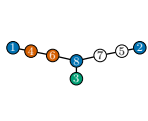
(58)

(3484, 4094, 192)



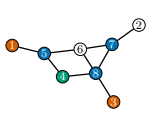
(59)

(2544, 5030, 196)



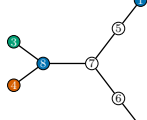
(60)

(3312, 4262, 196)



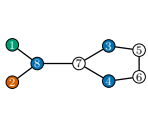
(61)

(2612, 4958, 200)



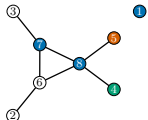
(62)

(3428, 4142, 200)



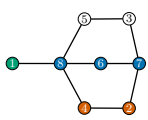
(63)

(2352, 5210, 208)



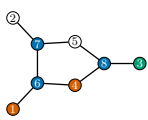
(64)

(4012, 3550, 208)

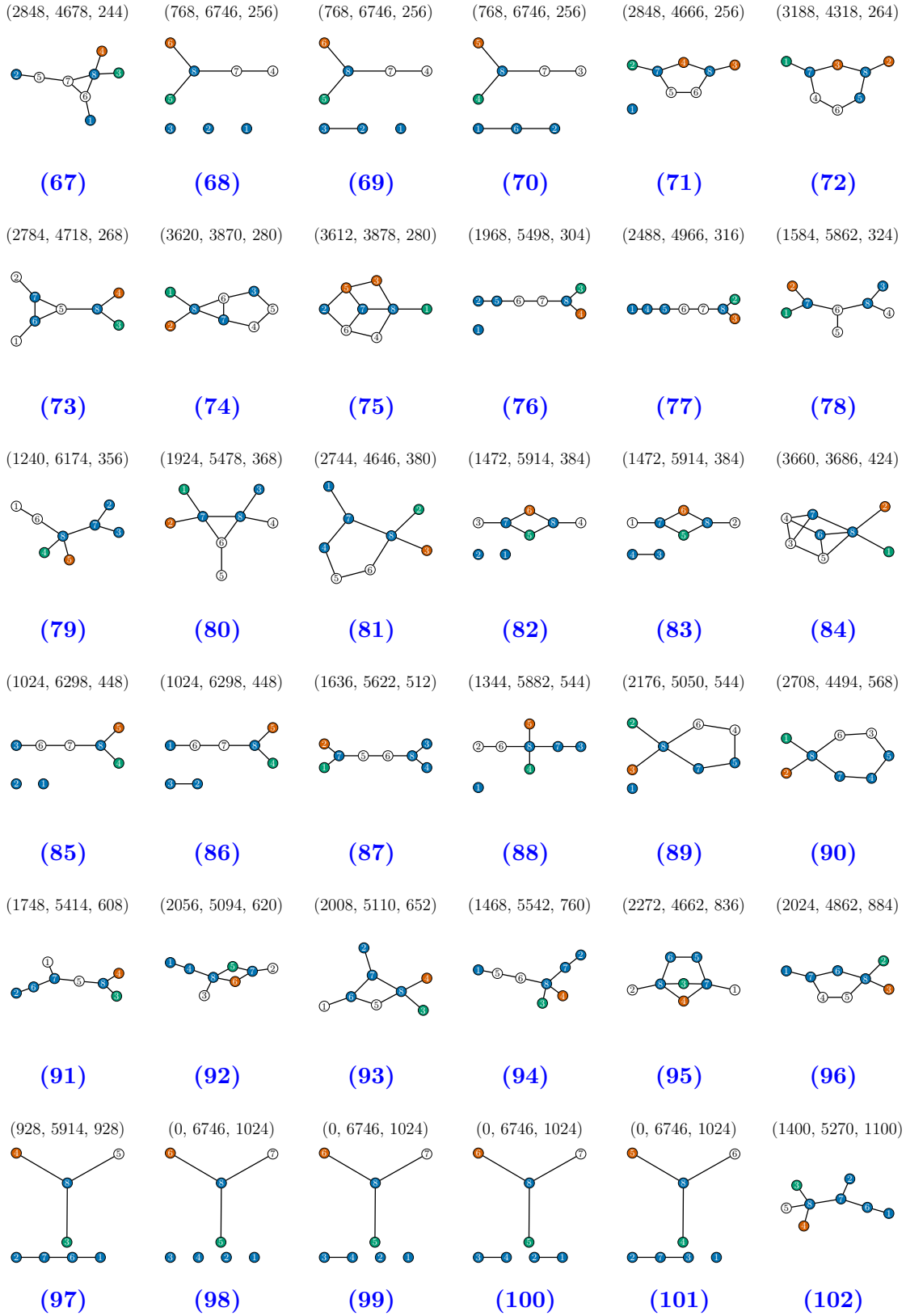


(65)

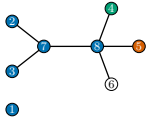
(2968, 4566, 236)



(66)

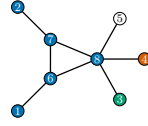


(336, 6298, 1136)



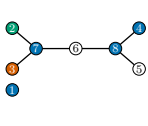
(103)

(1692, 4838, 1240)



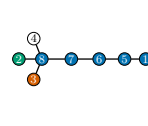
(104)

(672, 5818, 1280)



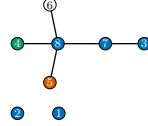
(105)

(1468, 4918, 1384)



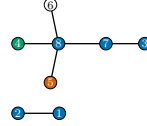
(106)

(448, 5914, 1408)



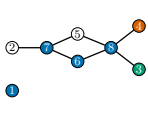
(107)

(448, 5914, 1408)



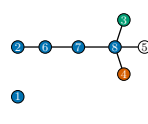
(108)

(912, 5402, 1456)



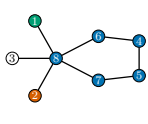
(109)

(576, 5498, 1696)



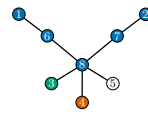
(110)

(1568, 4502, 1700)



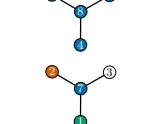
(111)

(752, 5222, 1796)



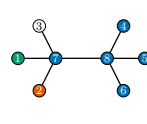
(112)

(0, 5818, 1952)

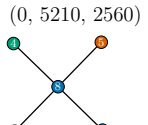


(113)

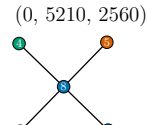
(196, 5574, 2000)



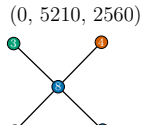
(114)



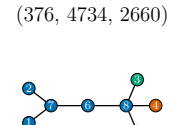
(115)



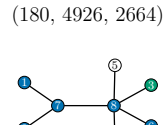
(116)



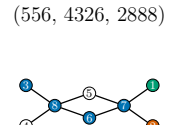
(117)



(118)

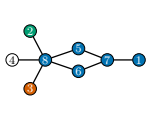


(119)



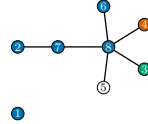
(120)

(500, 4326, 2944)



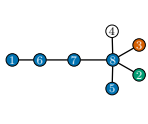
(121)

(240, 4570, 2960)



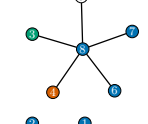
(122)

(304, 4206, 3260)



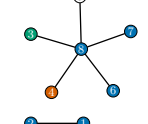
(123)

(0, 3610, 4160)



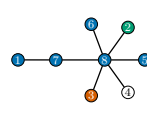
(124)

(0, 3610, 4160)

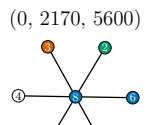


(125)

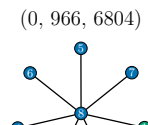
(124, 3126, 4520)



(126)

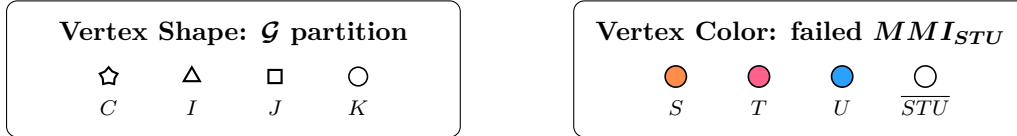


(127)



(128)

Table 12: Minimal-edge \mathcal{G} representatives of each entropy vector, unique up to symmetry at $n = 8$, corresponding to states that fail MMI_{CIJ} under the partition $\{C, I, J, K\}$ indicated by coloring. MMI evaluation counts are listed in the form (Satisfies, Saturates, Fails), each entry giving the MMI instance count yielding the respective outcome. Graphs are enumerated in increasing order of failed MMI instances, with edge count and graph diameter serving as tie-breakers, in that order. Notice that every graph shown contains an induced four-star.



Clicking each graph's label redirects to a website that provides easy access to the entropy vector of its state.

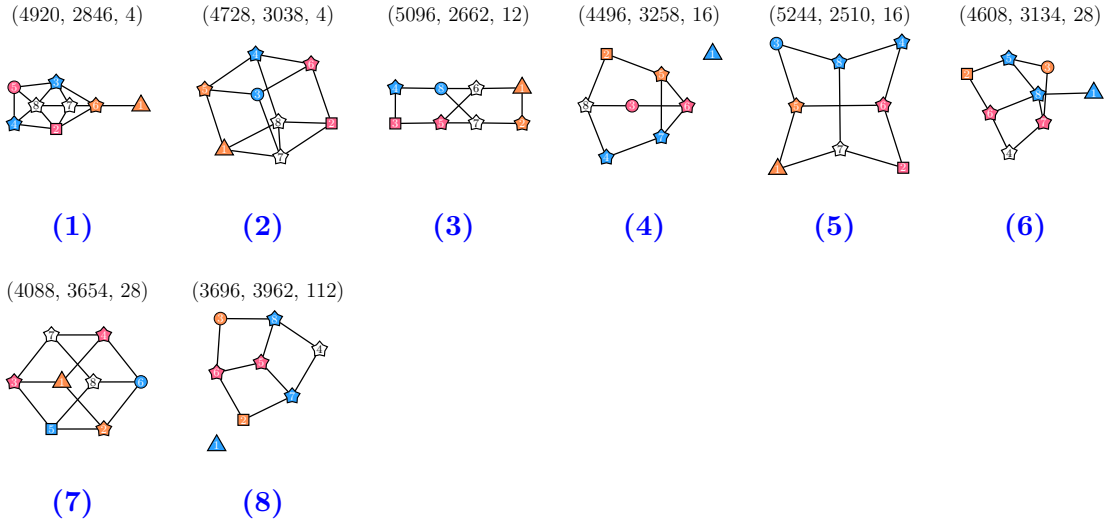


Table 13: Minimal-edge \mathcal{G} representatives of each entropy vector, unique up to symmetry at $n = 8$, corresponding to states that fail MMI but none of type MMI_{CIJ} . Vertex shape encodes a partition $\{C, I, J, K\}$ under which the graph is of type \mathcal{G} , while coloring indicates the partition $\{S, T, U, \overline{STU}\}$ under which the state fails MMI_{STU} . An exhaustive search of the LC orbit of each representative found no choices of $\{C, I, J\}$ such that the column spaces of CI , CJ , and CK intersected non-trivially. MMI evaluation counts are listed in the form (Satisfies, Saturates, Fails), each entry giving the MMI instance count yielding the respective outcome. Graphs are enumerated in increasing order of failed MMI instances, with edge count and graph diameter serving as tie-breakers, in that order. Notice that every graph shown contains an induced four-star.

B MMI Failure in Stabilizer States

For stabilizer state entropy vectors on $n \leq 5$ qubits, we also have a complete description for which entropy vectors saturate, satisfy, and fail MMI. In the following subsections we discuss the various instances of MMI that arise at each qubit number, and how each relates to the corresponding set of stabilizer entropy vectors.

Note: Instances of MMI which include all single-qubit subregions in the inequality are trivially satisfied by stabilizer states. There is therefore no need to check such instances.

B.0.1 Three Qubits

For $n = 3$ qubits there are 5 total stabilizer state entropy vectors, which reduce to 3 entropy vectors up to symmetry by qubit exchange. Table 14 gives a representative from each symmetry class, along with the number and percentage of overall states which have each entropy vector.

	A	B	C	Num. States
$s_{1,1,1}$	0	0	0	216 (20%)
$s_{2,1}$	1	1	0	432 (40%)
s_3	1	1	1	432 (40%)

Table 14. Stabilizer entropy vectors on 3 qubits, all trivially saturate MMI.

Vectors $s_{1,1,1}$ and $s_{2,1}$ in Table 14 correspond to product states of the form $A \otimes B \otimes C$ and $AB \otimes C$, respectively. Vector s_3 represents GHZ-type entanglement among 3 qubits. All vectors in Table 14 trivially saturate or satisfy the single 3-qubit instance of MMI.

B.0.2 Four Qubits

At 4 qubits, there are 18 stabilizer state entropy vectors which arrange into 6 equivalence classes up to qubit-exchange symmetry. Table 15 gives a single representative from each equivalence class, as well as the number of overall states which admit an entropy vector in each equivalence class.

The first 4 vectors in Table 15 are products of lower-qubit entropy vectors¹⁰, and thereby will trivially saturate all instances of MMI. Only s_{4_1} and s_{4_2} represent non-trivial entanglement among 4 qubits.

At 4 qubits there are 10 instances of MMI. We express each instance in the table below, where the sum of the left-hand columns must be greater than or equal to the sum of the right

¹⁰These vectors lie at the base of the MMI cone in some sense, since several of their components are 0.

	A	B	C	D	AB	AC	AD	Num. States	
$s_{1,1,1,1}$	0	0	0	0	0	0	0	1296	(3.53%)
$s_{2,1,1}$	1	1	0	0	0	1	1	5184	(14.11%)
$s_{3,1}$	1	1	1	0	1	1	1	10368	(28.24%)
$s_{2,2}$	1	1	1	1	0	2	2	1728	(4.71%)
s_{4_1}	1	1	1	1	1	1	1	2592	(7.1%)
s_{4_2}	1	1	1	1	1	2	2	15552	(42.35%)

Table 15. Representatives of the 6 equivalence classes, up to qubit exchange symmetry, for all 4-qubit stabilizer state entropy vectors.

$IJ + IK + JK \geq I + J + K + IJK$							
1	{A, B}	{A, C}	{B, C}	{A}	{B}	{C}	{A, B, C}
2	{A, B}	{A, D}	{B, D}	{A}	{B}	{D}	{A, B, D}
3	{A, C}	{A, D}	{C, D}	{A}	{C}	{D}	{A, C, D}
4	{B, C}	{B, D}	{C, D}	{B}	{C}	{D}	{B, C, D}

Table 16 below gives the data for all 4-qubit entropy vectors, stating whether each saturates, satisfies or fails MMI. Each column of Table 16 represents exactly one non-trivial instance of MMI, read from left to right (following top to bottom in the MMI instances table).

	1	2	3	4
$s_{1,1,1,1}$	S	S	S	S
$s_{2,1,1}$	S	S	S	S
$s_{3,1}$	S	S	S	S
$s_{2,2}$	S	S	S	S
s_{4_1}	F	F	F	F
s_{4_2}	Y	Y	Y	Y

Table 16. S = Saturates, Y = Satisfies, F = Fails.

We observe that vector s_{4_1} fails 4 instances of MMI, and so lives outside the MMI cone. Vector s_{4_2} lies inside the MMI cone, but does not saturate any non-trivial instance of MMI.

B.0.3 Five Qubits

At 5 qubits, the 93 stabilizer state entropy vectors reduce to the following 11 representatives

The first 7 entropy vectors of Table 17 are lifts of lower-qubit entanglement structures. The first 5 entropy vectors in particular are lifts of 3-qubit entanglement, and will trivially satisfy all 5-qubit instances of MMI.

		A		E	AB									DE	Num. States	
$s_{1,1,1,1,1}$	1	0	0	0	0	0	0	0	0	0	0	0	0	0	15552 (0.64%)	
$s_{2,1,1,1}$	10	1	1	0	0	0	1	1	1	1	1	1	0	0	160704 (6.63%)	
$s_{3,1,1}$	10	1	1	1	0	0	1	1	1	1	1	1	1	0	51840 (2.14%)	
$s_{2,2,1}$	15	1	1	1	1	0	0	2	2	1	2	2	1	0	1	400896 (16.54%)
$s_{3,2}$	10	1	1	1	1	1	1	1	2	2	1	2	2	2	0	556416 (22.96%)
$s_{4,1,1}$	5	1	1	1	1	0	1	1	1	1	1	1	1	1	1	63072 (2.60%)
$s_{4,2,1}$	15	1	1	1	1	0	1	2	2	1	2	2	1	1	1	273024 (11.27%)
s_{5_1}	1	1	1	1	1	1	1	1	1	1	1	1	1	1	1	15552 (0.64%)
s_{5_2}	10	1	1	1	1	1	1	2	2	2	2	2	2	1	1	362880 (14.97%)
s_{5_3}	15	1	1	1	1	1	1	2	2	2	2	2	2	1	2	513216 (21.18%)
s_{5_4}	1	1	1	1	1	1	2	2	2	2	2	2	2	2	2	10368 (0.43%)

Table 17. Representatives of the 11 equivalence classes, up to qubit exchange symmetry, for all 5-qubit stabilizer state entropy vectors.

Vectors $s_{4,1,1}$ and $s_{4,2,1}$ are lifts of entropy vectors s_{4_1} and s_{4_2} from Table 15. As with their 4-qubit analogs, the vectors $s_{4,1,1}$ and $s_{4,2,1}$ fail and satisfy, respectively, 5-qubit lifts of 4-qubit MMI.

The final four entropy vectors of Table 17 are genuine instances of 5-qubit entanglement. We discuss their relation to MMI below. At 5 qubits there are 40 unique instances of MMI, they are

$$\left(\begin{array}{ccc|ccc} \{A, B\} & \{A, O\} & \{B, O\} & \{A\} & \{B\} & \{O\} & \{A, B, O\} \\ \{A, B\} & \{A, D\} & \{B, D\} & \{A\} & \{B\} & \{D\} & \{A, B, D\} \\ \{A, B\} & \{A, C\} & \{B, C\} & \{A\} & \{B\} & \{C\} & \{A, B, C\} \\ \{A, C\} & \{A, O\} & \{C, O\} & \{A\} & \{C\} & \{O\} & \{A, C, O\} \\ \{A, C\} & \{A, D\} & \{C, D\} & \{A\} & \{C\} & \{D\} & \{A, C, D\} \\ \{A, D\} & \{A, O\} & \{D, O\} & \{A\} & \{D\} & \{O\} & \{A, D, O\} \\ \{B, C\} & \{B, O\} & \{C, O\} & \{B\} & \{C\} & \{O\} & \{B, C, O\} \\ \{B, C\} & \{B, D\} & \{C, D\} & \{B\} & \{C\} & \{D\} & \{B, C, D\} \\ \{B, D\} & \{B, O\} & \{D, O\} & \{B\} & \{D\} & \{O\} & \{B, D, O\} \\ \{C, D\} & \{C, O\} & \{D, O\} & \{C\} & \{D\} & \{O\} & \{C, D, O\} \end{array} \right)$$

{A, O}	{A, B, D}	{B, D, O}	{A}	{O}	{B, D}	{A, B, D, O}
{A, D}	{A, B, O}	{B, D, O}	{A}	{D}	{B, O}	{A, B, D, O}
{A, O}	{A, B, C}	{B, C, O}	{A}	{O}	{B, C}	{A, B, C, O}
{A, C}	{A, B, O}	{B, C, O}	{A}	{C}	{B, O}	{A, B, C, O}
{A, D}	{A, B, C}	{B, C, D}	{A}	{D}	{B, C}	{A, B, C, D}
{A, C}	{A, B, D}	{B, C, D}	{A}	{C}	{B, D}	{A, B, C, D}
{A, O}	{A, C, D}	{C, D, O}	{A}	{O}	{C, D}	{A, C, D, O}
{A, D}	{A, C, O}	{C, D, O}	{A}	{D}	{C, O}	{A, C, D, O}
{A, B}	{A, C, O}	{B, C, O}	{A}	{B}	{C, O}	{A, B, C, O}
{A, B}	{A, C, D}	{B, C, D}	{A}	{B}	{C, D}	{A, B, C, D}
{A, C}	{A, D, O}	{C, D, O}	{A}	{C}	{D, O}	{A, C, D, O}
{A, B}	{A, D, O}	{B, D, O}	{A}	{B}	{D, O}	{A, B, D, O}
{B, O}	{A, B, D}	{A, D, O}	{B}	{O}	{A, D}	{A, B, D, O}
{B, D}	{A, B, O}	{A, D, O}	{B}	{D}	{A, O}	{A, B, D, O}
{B, O}	{A, B, C}	{A, C, O}	{B}	{O}	{A, C}	{A, B, C, O}
{B, C}	{A, B, O}	{A, C, O}	{B}	{C}	{A, O}	{A, B, C, O}
{B, D}	{A, B, C}	{A, C, D}	{B}	{D}	{A, C}	{A, B, C, D}
{B, C}	{A, B, D}	{A, C, D}	{B}	{C}	{A, D}	{A, B, C, D}
{B, O}	{B, C, D}	{C, D, O}	{B}	{O}	{C, D}	{B, C, D, O}
{B, D}	{B, C, O}	{C, D, O}	{B}	{D}	{C, O}	{B, C, D, O}
{B, C}	{B, D, O}	{C, D, O}	{B}	{C}	{D, O}	{B, C, D, O}
{C, O}	{A, C, D}	{A, D, O}	{C}	{O}	{A, D}	{A, C, D, O}
{C, D}	{A, C, O}	{A, D, O}	{C}	{D}	{A, O}	{A, C, D, O}
{C, O}	{A, B, C}	{A, B, O}	{C}	{O}	{A, B}	{A, B, C, O}
{C, D}	{A, B, C}	{A, B, D}	{C}	{D}	{A, B}	{A, B, C, D}
{C, O}	{B, C, D}	{B, D, O}	{C}	{O}	{B, D}	{B, C, D, O}
{C, D}	{B, C, O}	{B, D, O}	{C}	{D}	{B, O}	{B, C, D, O}
{D, O}	{A, C, D}	{A, C, O}	{D}	{O}	{A, C}	{A, C, D, O}
{D, O}	{A, B, D}	{A, B, O}	{D}	{O}	{A, B}	{A, B, D, O}
{D, O}	{B, C, D}	{B, C, O}	{D}	{O}	{B, C}	{B, C, D, O}

Three-region MMI

B.0.4 Six Qubits

At 6 qubits there are 760 stabilizer state entropy vectors, which arrange into 26 equivalence symmetry classes up to qubit exchange. There are 15 lifts of lower-qubit entanglement and 11 new instances of 6-qubit entanglement.

	ABCDEF	A_	B_	C_	D_	EF	AB_	AC_	AD_	AEF
$S_{1,1,1,1,1,1}$	1	0 0 0 0 0 0	0 0 0 0 0	0 0 0 0	0 0 0	0 0	0 0 0 0	0 0 0	0 0 0	0 0 0
$S_{2,1,1,1,1}$	15	0 0 0 0 1 1	0 0 0 1 1	0 0 1 1	0 1 1	1 1	0 0 1 1	0 1 1	1 1 0	0 0 1 1
$S_{2,2,1,1}$	45	0 0 1 1 1 1	0 1 1 1 1	1 1 1 1	0 2 2	2 2	0 1 1 1 1	0 2 2	2 2 0	1 1 1 1
$S_{2,2,2}$	15	1 1 1 1 1 1	0 2 2 2 2	2 2 2 2	0 2 2	2 2	0 1 1 1 1	1 3 3	3 3 1	1 1 1 1
$S_{3,1,1,1}$	20	0 0 0 1 1 1	0 0 1 1 1	0 1 1 1	1 1 1	1 1	1 0 1 1 1	1 1 1	1 1 1	1 1 1 1
$S_{3,2,1}$	60	0 1 1 1 1 1	1 1 1 1 1	0 2 2 2	2 2 2	1 1	1 0 2 2 2	2 2 2	1 1 1	0 2 2 2
$S_{3,3}$	10	1 1 1 1 1 1	1 1 2 2 2	1 2 2 2	2 2 2	1 1	1 0 2 2 2	2 2 2	2 2 2	2 2 2
$S_{4,1,1,1}$	15	0 0 1 1 1 1	0 1 1 1 1	1 1 1 1	1 1 1	1 1	1 1 1 1 1	1 1 1	1 1 1	1 1 1 1
$S_{4,2,1,1}$	45	0 0 1 1 1 1	0 1 1 1 1	1 1 1 1	1 2 2	2 2	1 1 1 1 1	1 2 2	2 2 1	1 1 1 1
$S_{4,1,2}$	15	1 1 1 1 1 1	0 2 2 2 2	2 2 2 2	1 1 1	1 1	1 1 1 1 1	2 2 2	2 2 2	2 2 2
$S_{4,2,2}$	45	1 1 1 1 1 1	0 2 2 2 2	2 2 2 2	1 2 2	2 2	1 1 1 1 1	2 3 3	3 3 2	2 2 2
$S_{5,1,1}$	6	0 1 1 1 1 1	1 1 1 1 1	1 1 1 1	1 1 1	1 1	1 1 1 1 1	1 1 1	1 1 1	1 1 1 1
$S_{5,2,1}$	60	0 1 1 1 1 1	1 1 1 1 1	1 1 2 2	1 2 2	2 2	1 1 1 2 2	1 2 2	2 2 1	1 1 2 2
$S_{5,3,1}$	90	0 1 1 1 1 1	1 1 1 1 1	1 2 2 2	2 2 2	1 2	2 1 2 2 2	2 2 2	1 2 2	0 2 2 2
$S_{5,4,1}$	6	0 1 1 1 1 1	1 1 1 1 1	2 2 2 2	2 2 2	2 2	2 2 2 2 2	2 2 2	2 2 2	2 2 2 2
S_{6_1}	1	1 1 1 1 1 1	1 1 1 1 1	1 1 1 1	1 1 1	1 1	1 1 1 1 1	1 1 1	1 1 1	1 1 1 1
S_{6_2}	15	1 1 1 1 1 1	1 1 1 2 2	1 1 2 2	1 2 2	2 2	1 1 1 2 2	1 2 2	2 2 1	1 1 2 2
S_{6_3}	10	1 1 1 1 1 1	1 1 2 2 2	1 2 2 2	2 2 2	1 1	1 1 2 2 2	2 2 2	2 2 2	2 2 2
S_{6_4}	60	1 1 1 1 1 1	1 1 2 2 2	1 2 2 2	2 2 2	1 2	2 1 2 2 2	2 2 2	2 2 2	2 2 2
S_{6_5}	15	1 1 1 1 1 1	1 2 2 2 2	2 2 2 2	1 2 2	2 2	1 2 2 2 2	2 2 2	2 2 2	2 2 2
S_{6_6}	45	1 1 1 1 1 1	1 2 2 2 2	2 2 2 2	1 2 2	2 2	1 1 1 2 2	2 3 3	3 3 2	2 2 2
S_{6_7}	15	1 1 1 1 1 1	1 2 2 2 2	2 2 2 2	1 2 2	2 2	1 2 2 2 2	2 3 3	3 3 2	2 2 2
S_{6_8}	90	1 1 1 1 1 1	1 2 2 2 2	2 2 2 2	1 2 2	2 2	2 2 1 2 2	2 3 3	3 3 2	2 2 2
S_{6_9}	45	1 1 1 1 1 1	1 2 2 2 2	2 2 2 2	2 2 2	2 2	2 2 2 2 2	2 3 3	3 3 2	2 2 2
$S_{6_{10}}$	15	1 1 1 1 1 1	2 2 2 2 2	2 2 2 2	2 2 2	2 2	2 2 3 3	3 2 3	2 3 3	2 2 2
$S_{6_{11}}$	1	1 1 1 1 1 1	2 2 2 2 2	2 2 2 2	2 2 2	2 2	3 3 3 3	3 3 3	3 3 3	3 3 3

Figure 10. Representatives of the 26 equivalence classes, up to qubit exchange symmetry, for all 6-qubit stabilizer-state entropy vectors.

MMI \ Vec.

	S_{6_1}	S_{6_2}	S_{6_3}	S_{6_4}	S_{6_5}	S_{6_6}	S_{6_7}	S_{6_8}	S_{6_9}	$S_{6_{10}}$	$S_{6_{11}}$
(1,1,1)	{0, 0, 20}	{4, 12, 4}	{0, 18, 2}	{7, 12, 1}	{8, 12, 0}	{4, 16, 0}	{0, 20, 0}	{6, 14, 0}	{8, 12, 0}	{8, 12, 0}	{0, 20, 0}
(2,1,1)	{0, 0, 90}	{6, 48, 36}	{18, 72, 0}	{18, 60, 12}	{30, 48, 12}	{56, 32, 2}	{90, 0, 0}	{62, 28, 0}	{72, 16, 2}	{78, 12, 0}	{90, 0, 0}
(3,1,1)	{0, 0, 60}	{12, 36, 12}	{0, 54, 6}	{21, 36, 3}	{24, 36, 0}	{12, 48, 0}	{0, 60, 0}	{18, 42, 0}	{24, 36, 0}	{24, 36, 0}	{0, 60, 0}
(2,2,1)	{0, 0, 90}	{6, 48, 36}	{18, 72, 0}	{18, 60, 12}	{30, 48, 12}	{56, 32, 2}	{90, 0, 0}	{62, 28, 0}	{72, 16, 2}	{78, 12, 0}	{90, 0, 0}

{Y, S, F}

Figure 11. Table showing MMI satisfaction, saturation, and failure counts for all 6-qubit entanglement structures given in Table 10. Each row is determined by the partition that defines the MMI lift, e.g. (3,1,1). Each cell contains the triple $\{Y, S, F\}$, where Y counts the number of instances satisfied, S the number saturated, and F the number failed.

B.0.5 Seven Qubits

At 7 qubits there are 10773 stabilizer state entropy vectors, which arrange into 59 equivalence symmetry classes up to qubit exchange. There are 33 lifts of lower-qubit entanglement and 26 instances of 7-qubit entanglement. The sizes of each 7-qubit symmetry orbit are

$$\begin{aligned}
 &1, 1, 7, 7, 21, 21, 21, 21, 21, 21, 21, 21, 30, 35, 35, 35, 35, 70, 70, \\
 &70, 105, 105, 105, 105, 105, 105, 105, 105, 105, 105, 105, 105, 105, 105, \\
 &105, 105, 105, 105, 105, 210, 210, 210, 210, 210, 315, 315, 315, 315, 315, \\
 &315, 315, 315, 315, 315, 315, 360, 420, 420, 630, 630, 630, 630, 630.
 \end{aligned} \tag{B.1}$$

There are 26 new entanglement structures among the 7-qubit stabilizer states. Each is shown in Figure 12, listed alongside the size of their respective symmetry orbits under qubit exchange.

B.1 MMI Failure

We present data on MMI failure in stabilizer states through 6 qubits. We obtain a tableau representative for each stabilizer state, ignoring global phases, and compute the entropy vectors. The first three columns of Table 18 give the number of tableaux that saturate every MMI instance, those that do not fail any instance and satisfy at least one, and those that fail at least one MMI instance, respectively. The last column gives the number of entropy vectors at each qubit number that correspond to MMI-failing states. We account for global phases by multiplying the obtained counts by 2^n . All data is available and reproducible from *Mathematica* notebooks in [35, 63]

	ABCDEF	GH	A_	B_	C_	D_	E_	AB_	AC_	AD_	AE_	BC_	BD_	BE_	CD_	CE_	DE_	EFG
S_{7_1}	1	1	1	1	1	1	1	1	1	1	1	1	1	1	1	1	1	1
S_{7_2}	21	1	1	1	1	1	1	1	1	1	1	1	1	1	1	1	1	1
S_{7_3}	35	1	1	1	1	1	1	1	1	1	1	1	1	1	1	1	1	1
S_{7_4}	105	1	1	1	1	1	1	1	1	1	1	1	1	1	1	1	1	1
S_{7_5}	70	1	1	1	1	1	1	1	1	1	1	1	1	1	1	1	1	1
S_{7_6}	105	1	1	1	1	1	1	1	1	1	1	1	1	1	1	1	1	1
S_{7_7}	105	1	1	1	1	1	1	1	1	1	1	1	1	1	1	1	1	1
S_{7_8}	210	1	1	1	1	1	1	1	1	1	1	1	1	1	1	1	1	1
S_{7_9}	105	1	1	1	1	1	1	1	1	1	1	1	1	1	1	1	1	1
$S_{7_{10}}$	420	1	1	1	1	1	1	1	1	1	1	1	1	1	1	1	1	1
$S_{7_{11}}$	105	1	1	1	1	1	1	1	1	1	1	1	1	1	1	1	1	1
$S_{7_{12}}$	630	1	1	1	1	1	1	1	1	1	1	1	1	1	1	1	1	1
$S_{7_{13}}$	315	1	1	1	1	1	1	1	1	1	1	1	1	1	1	1	1	1
$S_{7_{14}}$	315	1	1	1	1	1	1	1	1	1	1	1	1	1	1	1	1	1
$S_{7_{15}}$	105	1	1	1	1	1	1	1	1	1	1	1	1	1	1	1	1	1
$S_{7_{16}}$	315	1	1	1	1	1	1	1	1	1	1	1	1	1	1	1	1	1
$S_{7_{17}}$	630	1	1	1	1	1	1	1	1	1	1	1	1	1	1	1	1	1
$S_{7_{18}}$	630	1	1	1	1	1	1	1	1	1	1	1	1	1	1	1	1	1
$S_{7_{19}}$	630	1	1	1	1	1	1	1	1	1	1	1	1	1	1	1	1	1
$S_{7_{20}}$	315	1	1	1	1	1	1	1	1	1	1	1	1	1	1	1	1	1
$S_{7_{21}}$	315	1	1	1	1	1	1	1	1	1	1	1	1	1	1	1	1	1
$S_{7_{22}}$	30	1	1	1	1	1	1	1	1	1	1	1	1	1	1	1	1	1
$S_{7_{23}}$	360	1	1	1	1	1	1	1	1	1	1	1	1	1	1	1	1	1
$S_{7_{24}}$	105	1	1	1	1	1	1	1	1	1	1	1	1	1	1	1	1	1
$S_{7_{25}}$	21	1	1	1	1	1	1	1	1	1	1	1	1	1	1	1	1	1
$S_{7_{26}}$	105	1	1	1	1	1	1	1	1	1	1	1	1	1	1	1	1	1

Figure 12. Novel entanglement structures first appearing at 7 qubits. Each entropy vector represents a symmetry orbit, under qubit exchange, the size of which is given in the second column.

MMI \ Vec.

	S_{7_1}	S_{7_2}	S_{7_3}	S_{7_4}	S_{7_5}	S_{7_6}	S_{7_7}	S_{7_8}	S_{7_9}
(1,1,1)	{0, 0, 35}	{5, 20, 10}	{0, 30, 5}	{9, 22, 4}	{9, 24, 2}	{12, 22, 1}	{6, 28, 1}	{2, 32, 1}	{0, 34, 1}
(2,1,1)	{0, 0, 210}	{10, 100, 100}	{12, 156, 42}	{24, 132, 54}	{24, 150, 36}	{30, 144, 36}	{48, 144, 18}	{61, 142, 7}	{78, 120, 12}
(3,1,1)	{0, 0, 210}	{10, 100, 100}	{12, 156, 42}	{24, 132, 54}	{24, 150, 36}	{30, 144, 36}	{48, 144, 18}	{61, 142, 7}	{78, 120, 12}
(4,1,1)	{0, 0, 105}	{15, 60, 30}	{0, 90, 15}	{27, 66, 12}	{27, 72, 6}	{36, 66, 3}	{18, 84, 3}	{6, 96, 3}	{0, 102, 3}
(2,2,1)	{0, 0, 315}	{0, 90, 225}	{27, 216, 72}	{9, 162, 144}	{27, 162, 126}	{45, 108, 162}	{90, 180, 45}	{153, 162, 0}	{207, 108, 0}
(2,2,2)	{0, 0, 105}	{0, 30, 75}	{9, 72, 24}	{3, 54, 48}	{9, 54, 42}	{15, 36, 54}	{30, 60, 15}	{51, 54, 0}	{69, 36, 0}
(3,2,1)	{0, 0, 420}	{20, 200, 200}	{24, 312, 84}	{48, 264, 108}	{48, 300, 72}	{60, 288, 72}	{96, 288, 36}	{122, 284, 14}	{156, 240, 24}

{Y, S, F}

MMI \ Vec.

	$S_{7_{10}}$	$S_{7_{11}}$	$S_{7_{12}}$	$S_{7_{13}}$	$S_{7_{14}}$	$S_{7_{15}}$	$S_{7_{16}}$	$S_{7_{17}}$	$S_{7_{18}}$
(1,1,1)	{6, 28, 1}	{10, 24, 1}	{7, 28, 0}	{5, 30, 0}	{9, 26, 0}	{3, 32, 0}	{1, 34, 0}	{7, 28, 0}	{5, 30, 0}
(2,1,1)	{66, 132, 12}	{72, 120, 18}	{81, 126, 3}	{94, 112, 4}	{94, 110, 6}	{102, 108, 0}	{114, 96, 0}	{104, 106, 0}	{118, 90, 2}
(3,1,1)	{66, 132, 12}	{72, 120, 18}	{81, 126, 3}	{94, 112, 4}	{94, 110, 6}	{102, 108, 0}	{114, 96, 0}	{104, 106, 0}	{118, 90, 2}
(4,1,1)	{18, 84, 3}	{30, 72, 3}	{21, 84, 0}	{15, 90, 0}	{27, 78, 0}	{9, 96, 0}	{3, 102, 0}	{21, 84, 0}	{15, 90, 0}
(2,2,1)	{153, 144, 18}	{162, 108, 45}	{177, 126, 12}	{219, 90, 6}	{225, 60, 30}	{258, 54, 3}	{297, 18, 0}	{225, 90, 0}	{267, 48, 0}
(2,2,2)	{51, 48, 6}	{54, 36, 15}	{59, 42, 4}	{73, 30, 2}	{75, 20, 10}	{86, 18, 1}	{99, 6, 0}	{75, 30, 0}	{89, 16, 0}
(3,2,1)	{132, 264, 24}	{144, 240, 36}	{162, 252, 6}	{188, 224, 8}	{188, 220, 12}	{204, 216, 0}	{228, 192, 0}	{208, 212, 0}	{236, 180, 4}

{Y, S, F}

MMI \ Vec.

	$S_{7_{19}}$	$S_{7_{20}}$	$S_{7_{21}}$	$S_{7_{22}}$	$S_{7_{23}}$	$S_{7_{24}}$	$S_{7_{25}}$	$S_{7_{26}}$
(1,1,1)	{8, 27, 0}	{7, 28, 0}	{4, 31, 0}	{7, 28, 0}	{7, 28, 0}	{7, 28, 0}	{0, 35, 0}	{3, 32, 0}
(2,1,1)	{120, 88, 2}	{134, 76, 0}	{146, 64, 0}	{126, 84, 0}	{161, 49, 0}	{156, 54, 0}	{150, 60, 0}	{174, 36, 0}
(3,1,1)	{120, 88, 2}	{134, 76, 0}	{146, 64, 0}	{126, 84, 0}	{161, 49, 0}	{156, 54, 0}	{150, 60, 0}	{174, 36, 0}
(4,1,1)	{24, 81, 0}	{21, 84, 0}	{12, 93, 0}	{21, 84, 0}	{21, 84, 0}	{21, 84, 0}	{0, 105, 0}	{9, 96, 0}
(2,2,1)	{255, 54, 6}	{282, 30, 3}	{309, 6, 0}	{294, 0, 21}	{294, 21, 0}	{306, 0, 9}	{315, 0, 0}	{312, 0, 3}
(2,2,2)	{85, 18, 2}	{94, 10, 1}	{103, 2, 0}	{98, 0, 7}	{98, 7, 0}	{102, 0, 3}	{105, 0, 0}	{104, 0, 1}
(3,2,1)	{240, 176, 4}	{268, 152, 0}	{292, 128, 0}	{252, 168, 0}	{322, 98, 0}	{312, 108, 0}	{300, 120, 0}	{348, 72, 0}

{Y, S, F}

Figure 13. MMI table for 7-qubit entanglement structures given from Table 12. Each row is labeled by the partition that defines that MMI lift, e.g. (3,2,1). The value Y counts the number of satisfied instances, S the number saturated, and F the number failed.

Qubit #	MMI			Ent. Vec. Fail
	Satur.	Satis.	Fail	
3	1,080 (100%)	0 (0%)	0 (0%)	(0%)
4	18,576 (50.6%)	15,552 (42.36%)	2,592 (7.06%)	1 (5.55%)
5	370,656 (15.29%)	1,648,512 (68%)	404,352 (16.70%)	16 (17.20%)
6	9,118,656 (2.89%)	175,115,520 (55.59%)	130,823,424 (41.52%)	287 (37.76%)
7	-	-	-	6436 (59.74%)

Table 18. State and vector count for totally saturate, at least satisfy, and (at least 1 instance) fail MMI.

References

- [1] M. Walter, D. Gross and J. Eisert, *Multipartite entanglement*, *arXiv preprint arXiv:1612.02437* (2016) .
- [2] G. Vidal and R.F. Werner, *Computable measure of entanglement*, *Phys. Rev. A* **65** (2002) 032314.
- [3] R. Horodecki, P. Horodecki, M. Horodecki and K. Horodecki, *Quantum entanglement*, *Rev. Mod. Phys.* **81** (2009) 865.
- [4] V. Coffman, J. Kundu and W.K. Wootters, *Distributed entanglement*, *Phys. Rev. A* **61** (2000) 052306.
- [5] N. Linden, S. Popescu, J.A. Smolin and F. Verstraete, *Entanglement of formation and distillable entanglement of multipartite mixed states*, *Phys. Rev. Lett.* **89** (2002) 207901.
- [6] E.H. Lieb and M.B. Ruskai, *Proof of the strong subadditivity of quantum-mechanical entropy*, *Journal of Mathematical Physics* **14** (1973) 1938.
- [7] E.H. Lieb, *Convex trace functions and the wigner–yanase–dyson conjecture*, *Advances in Mathematics* **11** (1973) 267.
- [8] E.A. Carlen, R.L. Frank and E.H. Lieb, *Some operator and trace function convexity theorems*, [1409.0564](#).
- [9] N. Linden, F. Matúš, M.B. Ruskai and A. Winter, *The quantum entropy cone of*

- stabiliser states, *in: Proc. 8th TQC Guelph, LIPICS vol. 22, pp. 270-284, 2013* (2013) [[1302.5453](#)].
- [10] Z. Zhang and R. Yeung, *A non-shannon-type conditional inequality of information quantities*, *IEEE Transactions on Information Theory* **43** (1997) 1982.
- [11] N. Lashkari, C. Rabideau, P. Sabella-Garnier and M. Van Raamsdonk, *Inviolable energy conditions from entanglement inequalities*, *JHEP* **06** (2015) 067 [[1412.3514](#)].
- [12] Z. Zhang and R. Yeung, *On characterization of entropy function via information inequalities*, *IEEE Transactions on Information Theory* **44** (1998) 1440–1452.
- [13] F. Matús, *Infinitely many information inequalities*, *2007 IEEE International Symposium on Information Theory* (2007) 41.
- [14] R. Dougherty, C. Freiling and K. Zeger, *Networks, matroids, and non-shannon information inequalities*, *IEEE Transactions on Information Theory* **53** (2007) 1949.
- [15] N. Linden and A. Winter, *A new inequality for the von neumann entropy*, *Communications in Mathematical Physics* **259** (2005) 129–138.
- [16] S. Hernández-Cuenca, V.E. Hubeny and H.F. Jia, *Holographic entropy inequalities and multipartite entanglement*, *Journal of High Energy Physics* **2024** (2024) .
- [17] P. Hayden, M. Headrick and A. Maloney, *Holographic mutual information is monogamous*, *Phys. Rev. D* **87** (2013) 046003 [[1107.2940](#)].
- [18] J.M. Maldacena, *The Large N limit of superconformal field theories and supergravity*, *Adv. Theor. Math. Phys.* **2** (1998) 231 [[hep-th/9711200](#)].
- [19] N. Bao, S. Nezami, H. Ooguri, B. Stoica, J. Sully and M. Walter, *The holographic entropy cone*, *JHEP* **2015** (2015) 130.
- [20] N. Bao, N. Cheng, S. Hernández-Cuenca and V.P. Su, *A Gap Between the Hypergraph and Stabilizer Entropy Cones*, [2006.16292](#).
- [21] C. Keeler, W. Munizzi and J. Pollack, *Entropic lens on stabilizer states*, *Phys. Rev. A* **106** (2022) 062418 [[2204.07593](#)].
- [22] P. Hayden, M. Headrick and A. Maloney, *Holographic mutual information is monogamous*, *Phys. Rev. D* **87** (2013) 046003.
- [23] M. Hein, J. Eisert and H.J. Briegel, *Multipartite entanglement in graph states*, *Phys. Rev. A* **69** (2004) 062311.
- [24] M. Hein, W. Dür, J. Eisert, R. Raussendorf, M. Van den Nest and H.J. Briegel, *Entanglement in graph states and its applications*, [quant-ph/0602096](#).
- [25] D. Gottesman, *The heisenberg representation of quantum computers*, 1998.
- [26] S. Aaronson and D. Gottesman, *Improved simulation of stabilizer circuits*, *Phys. Rev. A* **70** (2004) 052328.
- [27] M. Van den Nest, J. Dehaene and B. De Moor, *Graphical description of the action of*

- local clifford transformations on graph states, *Physical Review A* **69** (2004) 022316 [quant-ph/0308151].
- [28] H.J. Briegel and R. Raussendorf, *Persistent entanglement in arrays of interacting particles*, *Physical Review Letters* **86** (2001) 910 [quant-ph/0004051].
- [29] R. Raussendorf and H.J. Briegel, *A one-way quantum computer*, *Physical Review Letters* **86** (2001) 5188 [quant-ph/0010033].
- [30] D. Fattal, T.S. Cubitt, Y. Yamamoto, S. Bravyi and I.L. Chuang, *Entanglement in the stabilizer formalism*, 2004.
- [31] B. Lovitz and N. Johnston, *Entangled subspaces and generic local state discrimination with pre-shared entanglement*, *Quantum* **6** (2022) 760.
- [32] W. Munizzi and H.J. Schnitzer, *Entropy Cones and Entanglement Evolution for Dicke States*, **2306.13146**.
- [33] C. Keeler, W. Munizzi and J. Pollack, *Clifford orbits from cayley graph quotients*, *Quant. Inf. Comput.* **24** (2024) 1 [2306.01043].
- [34] A. Burchardt and F. Hahn, *The foliage partition: An easy-to-compute lc-invariant for graph states*, 2025.
- [35] J. Fuentes and W. Munizzi, “Mmi-failure-for-graph-states.” <https://github.com/jesus99222/MMI-Failure-For-Graph-States>, 2025.
- [36] L.E. Danielsen and M.G. Parker, *On the classification of all self-dual additive codes over $gf(4)$ of length up to 12*, *Journal of Combinatorial Theory, Series A* **113** (2006) 1351–1367.
- [37] B. Czech and Y. Wang, *A holographic inequality for $N = 7$ regions*, *JHEP* **01** (2023) 101 [2209.10547].
- [38] T. He, V.E. Hubeny and M. Rangamani, *Superbalance of Holographic Entropy Inequalities*, *JHEP* **07** (2020) 245 [2002.04558].
- [39] C. Keeler, W. Munizzi and J. Pollack, *Bounding entanglement entropy with clifford double cosets*, *Physical Review A* **112** (2025) .
- [40] G. Salton, B. Swingle and M. Walter, *Entanglement from Topology in Chern-Simons Theory*, *Phys. Rev. D* **95** (2017) 105007 [1611.01516].
- [41] W. Munizzi and H.J. Schnitzer, *Topological Preparation of Non-Stabilizer States and Clifford Evolution in $SU(2)_1$ Chern-Simons Theory*, **2510.15067**.
- [42] J. Pollack and D. VanAllen, *Towards Entropic Constraints on Quantum Speedups*, **2411.03439**.
- [43] L. Leone, S.F.E. Oliviero and A. Hamma, *Stabilizer Rényi Entropy*, *Phys. Rev. Lett.* **128** (2022) 050402 [2106.12587].
- [44] N. Bao, C. Cao and V.P. Su, *Magic state distillation from entangled states*, *Phys. Rev. A* **105** (2022) 022602.

- [45] E. Dallas and P. Zanardi, *Nonlocal Magic Generation and Information Scrambling in Noisy Clifford Circuits*, [2509.20566](#).
- [46] J. De Boer, J. Järvelä and E. Keski-Vakkuri, *Aspects of capacity of entanglement*, *Phys. Rev. D* **99** (2019) 066012 [[1807.07357](#)].
- [47] C. Cao, G. Cheng, A. Hamma, L. Leone, W. Munizzi and S.F.E. Oliviero, *Gravitational back-reaction is magical*, [2403.07056](#).
- [48] N. Khumalo, A. Mehta, W. Munizzi and P. Narang, *Navigating the Quantum Resource Landscape of Entropy Vector Space Using Machine Learning and Optimization*, [2511.16724](#).
- [49] F. Andreadakis and P. Zanardi, *An Exact Link between Nonlocal Magic and Operator Entanglement*, [2504.09360](#).
- [50] D.G. Fon-Der-Flaass, *Local complementations of simple and directed graphs*, in *Discrete Analysis and Operations Research*, A.D. Korshunov, ed., (Dordrecht), pp. 15–34, Springer Netherlands (1996), [DOI](#).
- [51] D. Kim and S. il Oum, *Vertex-minors of graphs: A survey*, *Discrete Applied Mathematics* **351** (2024) 54.
- [52] F. Hahn, A. Pappa and J. Eisert, *Quantum network routing and local complementation*, *npj Quantum Information* **5** (2019) .
- [53] V. Mannalath and A. Pathak, *Multiparty entanglement routing in quantum networks*, *Phys. Rev. A* **108** (2023) 062614 [[2211.06690](#)].
- [54] A. Sen, K. Goodenough and D. Towsley, *Multipartite Entanglement in Quantum Networks Using Subgraph Complementations*, in *2023 International Conference on Quantum Computing and Engineering*, 8, 2023, [DOI \[2308.13700\]](#).
- [55] K. Azuma, S.E. Economou, D. Elkouss, P. Hilaire, L. Jiang, H.-K. Lo et al., *Quantum repeaters: From quantum networks to the quantum internet*, *Rev. Mod. Phys.* **95** (2023) 045006 [[2212.10820](#)].
- [56] R. Negrin, N. Dirnegger, W. Munizzi, J. Talukdar and P. Narang, *Efficient multiparty entanglement distribution with DODAG-X protocol*, *Proc. SPIE Int. Soc. Opt. Eng.* **13391** (2025) 1339109 [[2408.07118](#)].
- [57] E. Hughes, W. Munizzi and P. Narang, *Improved Simulation of Asynchronous Entanglement Distribution in Noisy Quantum Networks*, [2507.22992](#).
- [58] P.W. Shor and J. Preskill, *Simple proof of security of the bb84 quantum key distribution protocol*, *Physical Review Letters* **85** (2000) 441–444.
- [59] D. Gottesman, H.-K. Lo, N. Lutkenhaus and J. Preskill, *Security of quantum key distribution with imperfect devices*, *Quant. Inf. Comput.* **4** (2004) 325 [[quant-ph/0212066](#)].
- [60] C.H. Bennett and G. Brassard, *Quantum cryptography: Public key distribution and coin tossing*, *Theor. Comput. Sci.* **560** (2014) 7 [[2003.06557](#)].

- [61] L. Mariani, R. Yehia, C. Pascual-García, F. Centrone, J. van der Kolk, M.Á. Serrano et al., *Quantum Key Distribution over Complex Networks*, [2504.02372](#).
- [62] A. Polishchuk and L. Positselski, *Quadratic Algebras*, vol. 37 of *University Lecture Series*, American Mathematical Society, Providence, RI (2005).
- [63] W. Munizzi, “Stabilizer-States.”
<https://github.com/WMunizzi/Stabilizer-States>, 4, 2022.
10.13140/RG.2.2.35482.41928.